

AFIT/GEO/ENG/93D-03

1

AD-A274 076



S DTIC
ELECTE
DEC 27 1993
A

**OPTICAL WAVELET TRANSFORM
FOR
FINGERPRINT IDENTIFICATION**

THESIS
Robert P. MacDonald
Captain, USAF

AFIT/GEO/ENG/93D-03

93-31030



7980

Approved for public release; distribution unlimited

93 12 22 1 43

**OPTICAL WAVELET TRANSFORM
FOR
FINGERPRINT IDENTIFICATION**

THESIS

**Presented to the Faculty of the Graduate School of Engineering
of the Air Force Institute of Technology**

Air University

**In Partial Fulfillment of the
Requirements for the Degree of
Master of Science in Electrical Engineering**

Robert P. MacDonald, B.S.E.E.

Captain, USAF

15 December, 1993

DTIC QUALITY INSPECTED 8

Approved for public release; distribution unlimited

Accession For	
NTIS	CRA&I <input checked="" type="checkbox"/>
DTIC	TAB <input type="checkbox"/>
Unannounced	<input type="checkbox"/>
Justification	
By	
Distribution/	
Availability Codes	
Dist	Avail and/or Special
A-1	

Preface

I can honestly say that while working on this thesis, I spent a good portion of that time in the dark, both literally making holograms and figuratively searching for a clue. I could not have accomplished anything without the support of others. I would like to recognize the following individuals for their guidance. My committee members, Dr. Greg Warhola and Dr. Dennis Ruck for their insights. Dr. Steve Rogers, who fortunately for AFIT and my research, decided to stay on as a civilian professor here at AFIT. For that matter I should thank the Dean for making the moves to retain Dr. Rogers' talents here. Hopefully many more future students will benefit from his mentoring. Dr Byron Welsh for his enthusiasm about my research. And I would especially like to thank Captain (soon to be Dr.) Ken Fielding and Captain (all but hooded, Dr.) Tom Burns for their combined wisdom, without which I would have remained within that caliginous region of unenlightenment.

This research has been a great experience, one that I will always remember fondly. There were various moments of despair, but with the support from the "back of the lab club", specifically Gary Shartle, Kim McCrae, John Keller, Neale Prescott, Curtis Martin, and Martin Chin, those moments were bearable. I would also like to thank Jo Jo for her continued encouragement and wish her good fortune in her scholastic endeavors.

MAC

Robert P. MacDonald

Table of Contents

	Page
Preface	ii
List of Figures	v
Abstract	viii
 I. Introduction	 1
1.1 Summary of Current Knowledge	1
1.2 Problem Statement	3
1.3 Scope	3
1.4 Outline of Thesis	3
 II. Literature Review	 5
2.1 Background	5
2.2 Transformation Techniques	5
2.2.1 Fourier Methods	5
2.2.2 Wavelet Methods	6
2.2.3 Analytical Comparison	8
2.2.4 Experimental Comparison	8
2.2.5 Symmetric Wavelet Transform	9
 III. Methodology	 12
3.1 Wavelet Filter	12
3.1.1 Mathematical Development of Wavelet and Basis Filters	 13
3.1.2 Binary Detour Phase Hologram	16
3.1.3 Two Dimensional Filters	20

	Page
3.2 Optical Architecture	26
3.3 Optical Wavelet Fingerprint Identification	29
3.3.1 Vander Lugt Filter	29
IV. Results	32
4.1 Characterization of Optical Biorthogonal Wavelet Transform	32
4.1.1 Input Image of Letter "E"	32
4.1.2 Horizontal Filter Results	32
4.1.3 Vertical Filter Results	36
4.1.4 Diagonal Filter Results	36
4.2 Optical Biorthogonal Wavelet Transform of Lenna	41
4.3 Optical Biorthogonal Wavelet Transform of a Fingerprint .	42
4.4 Improved Optical Wavelet Fingerprint Identifier	51
4.5 Test for Rotational Invariance	53
4.6 Summary	59
V. Conclusions	60
5.1 Future Applications	60
5.2 Recommendations	61
Appendix A. C Program used to Create Detour Phase Computer Gener- ated Hologram	62
Bibliography	66
Vita	68

List of Figures

Figure	Page
1. Two Dimensional Decomposition Algorithm (1)	7
2. One Dimensional Two-Channel Subband Coder	10
3. Diagram of Optical Correlator	12
4. Basis function $\phi(x)$ and its Fourier spectrum $\phi(\hat{x})$	15
5. Wavelet function $\psi(x)$ and the magnitude of its Fourier spectrum $\psi(\hat{x})$	15
6. Sample Cell of Detour Phase Hologram (30)	17
7. Transparency of Detour Phase Hologram	21
8. Dekacon Camera System	22
9. Horizontal Wavelet Filter: $\phi(\hat{x})\psi(\hat{y})$	23
10. Vertical Wavelet Filter: $\psi(\hat{x})\phi(\hat{y})$	24
11. Diagonal Wavelet Filter: $\psi(\hat{x})\psi(\hat{y})$	25
12. Adjustable Scale Optical Correlator	26
13. Improved Optical Wavelet Fingerprint Identification Arrangement	28
14. Vander Lugt Filter (18)	29
15. HC-500 Thermoplastic Recording Process (24)	31
16. Capital Letter "E"	33
17. Optical Wavelet Transform for Horizontal Filter on Letter E, $m = 0$ Resolution	34
18. Digital Wavelet Transform for Horizontal Filter on Letter E, $m = 0$ Resolution	34
19. Optical Wavelet Transform for Horizontal Filter on Letter E, $m = 1$ Resolution	35
20. Digital Wavelet Transform for Horizontal Filter on Letter E, $m = 1$ Resolution	35
21. Optical Wavelet Transform for Vertical Filter on Letter E, $m = 0$ Res- olution	37

Figure	Page
22. Digital Wavelet Transform for Vertical Filter on Letter E, $m = 0$ Resolution	37
23. Optical Wavelet Transform for Vertical Filter on Letter E, $m = 1$ Resolution	38
24. Digital Wavelet Transform for Vertical Filter on Letter E, $m = 1$ Resolution	38
25. Optical Wavelet Transform for Diagonal Filter on Letter E, $m = 0$ Resolution	39
26. Digital Wavelet Transform for Diagonal Filter on Letter E, $m = 0$ Resolution	39
27. Optical Wavelet Transform for Diagonal Filter on Letter E, $m = 1$ Resolution	40
28. Digital Wavelet Transform for Diagonal Filter on Letter E, $m = 1$ Resolution	40
29. Lenna	41
30. Horizontal Wavelet Transform Results for Lenna: (a) $m = 0$ (b) $m = 1$ (c) $m = 2$	43
31. Vertical Wavelet Transform Results for Lenna: (a) $m = 0$ (b) $m = 1$ (c) $m = 2$	44
32. Diagonal Wavelet Transform Results for Lenna: (a) $m = 0$ (b) $m = 1$ (c) $m = 2$	45
33. Fingerprint	46
34. Horizontal Wavelet Transform Results for Fingerprint: (a) $m = 0$ (b) $m = 1$ (c) $m = 2$	48
35. Vertical Wavelet Transform Results for Fingerprint: (a) $m = 0$ (b) $m = 1$ (c) $m = 2$	49
36. Diagonal Wavelet Transform Results for Fingerprint: (a) $m = 0$ (b) $m = 1$ (c) $m = 2$	50
37. Improved Optical Wavelet Fingerprint Identifier Results: Discrimination Against Subject 1 MSF	52

Figure	Page
38. Auto-Correlation Peak vs Offset Rotation for Normal and Wavelet Transformed Fingerprint Image at Various Rotations	54
39. Comparison of (a) Five Degree Offset Wavelet Auto-correlation and (b) Non-Rotated Subject Two Wavelet Cross-correlation with Subject One	55
40. MSF Correlation Peak Plot for Normal Non-Rotated Fingerprint . .	56
41. MSF Correlation Peak Plot for Wavelet Transformed Non-Rotated Fingerprint	56
42. MSF Correlation Peak Plot for Normal 3 Degree Offset Fingerprint .	57
43. MSF Correlation Peak Plot for Wavelet Transformed 3 Degree Offset Fingerprint	57
44. MSF Correlation Peak Plot for Normal 5 Degree Offset Fingerprint .	58
45. MSF Correlation Peak Plot for Wavelet Transformed 5 Degree Offset Fingerprint	58

Abstract

The Federal Bureau of Investigation (FBI) has recently sanctioned a wavelet fingerprint image compression algorithm developed for reducing storage requirements of digitized fingerprints. This research implements an optical wavelet transform of a fingerprint image, as the first step in an optical fingerprint identification process. Wavelet filters are created from computer generated holograms of biorthogonal wavelets, the same wavelets implemented in the FBI algorithm. Using a detour phase holographic technique, a complex binary filter mask is created with both symmetry and linear phase. The wavelet transform is implemented with continuous shift using an optical correlation between binarized fingerprints written on a Magneto-Optic Spatial Light Modulator (MOSLM) and the biorthogonal wavelet filters. A telescopic lens combination scales the transformed fingerprint onto the filters, providing a means of adjusting the biorthogonal wavelet filter dilation continuously. The wavelet transformed fingerprint is then applied to an optical fingerprint identification process. Comparison between normal fingerprints and wavelet transformed fingerprints shows improvement in the optical identification process, in terms of rotational invariance.

OPTICAL WAVELET TRANSFORM FOR FINGERPRINT IDENTIFICATION

I. Introduction

Automatic, real-time, personal identification is an important capability in a security conscious environment. In an age of almost unlimited access of information through computer networks, controlled access through automated recognition could maintain control with limited oversight of facilities. Whether for securing access to vital areas or assuring proper use of computer systems, this technology is a requirement. Law enforcement agencies use the uniqueness of the fingerprint for identifying and tracking criminals. The fingerprint remains as one of the constants against which personal identity can be matched. A security system can take advantage of this uniqueness for controlling access. Optics provide a method of implementing a fingerprint identification scheme in real-time. This research affects an optical fingerprint identifier with improvement in terms of rotational invariance.

1.1 Summary of Current Knowledge

An optical correlation is an effective method for discriminating fingerprints. This procedure has been implemented real-time using a 90-degree prism and a Magneto-Optic Spatial Light Modulator (MOSLM) (12). The advantage of this configuration is the compactness of the design stemming from a 1- f joint transform correlator. The MOSLM presents both the input fingerprint read in on the prism and the print to be matched against, making the design easy to implement in a compact portable form. However, this configuration is very sensitive to rotational alignment of the input print on the prism. It has been shown that the correlation

peak for fingerprint images drops off greater than 3 dB for alignment offsets greater than $\pm 1.5^\circ$ (14). This is due to the limited rotational symmetry in the fingerprint. Extraction of rotationally symmetric fingerprint features would help to alleviate this problem, as long as those features still contain enough uniqueness for discrimination.

The uniqueness of the fingerprint image lies in the construction of the ridges. Law enforcement agencies single out points where the ridges intersect and label them minutiae points. These minutiae points are then used for identifying the owner of the fingerprint. However, the uniqueness of the fingerprint is not limited to the ridge layout. There are finer details which are as distinctive as the minutiae points; the size and shape of the pores for instance (16). Since pore shapes are circular, they can be considered rotationally symmetric. An image processing routine which emphasized those symmetric, unique features would contribute towards circular symmetry.

One such routine is the wavelet transform. The wavelet transform translates signals into a time(space)-frequency representation. Representing image data using the wavelet transform allows localization of image spectrum content. The wavelet transform is readily implemented through correlation of the input image and a wavelet filter. For this reason, the wavelet transform has become a useful tool in optical image processing (27, 13, 21). The wavelet transformation of a two-dimensional input function, $f(x, y)$ is represented by:

$$W_h f(a, b, c, d) = \int \int_{-\infty}^{\infty} f(x, y) \frac{1}{\sqrt{ab}} h\left(\frac{x-c}{a}, \frac{y-d}{b}\right) dx dy \quad (1)$$

Where $h(\frac{x-c}{a}, \frac{y-d}{b})$ represents the two dimensional scaled and shifted "mother" wavelet.

The wavelet transform has been used for detection of objects in a 2-D scene (10). Because the wavelet transform is an effective edge detector, it suppressed background clutter and emphasized the target image's edges. The fingerprint image

is merely a series of "edges". In the same manner the wavelet transform can be used for emphasizing the rotationally symmetric details of a fingerprint image.

1.2 Problem Statement

This thesis implements an optical wavelet transform on a fingerprint image to enhance the identification process.

1.3 Scope

This research augments fingerprint identification, accomplishable in two phases. The first phase optically computes the wavelet transform of images for storage. Results of the optical wavelet transform are compared to results of previous research. The second phase is an optical correlation between wavelet transformed fingerprint images for identification. The wavelet transformed fingerprint is examined for identification uniqueness and rotational tolerance. This research does not explore alternative methods of matching fingerprints. There is no attempt to perform feature extraction on the fingerprint image for classification through standard pattern recognition algorithms. Feature extraction, a process of identifying those features which make the image unique, emphasizes a different research area.

1.4 Outline of Thesis

This document is organized as follows. Chapter II provides the background which lead to the decision to focus this research on fingerprint analysis. The symmetric biorthogonal wavelet transform is discussed as the objective of this research. Chapter III presents the various technologies involved in this research. Two methods of creating a hologram are presented in detail. The results are presented in Chapter IV. The optical biorthogonal wavelet transform is characterized using three images for transformation. Results from an optical identifier are also presented. Finally,

Chapter V presents conclusions and recommendations for future research in this area.

II. Literature Review

2.1 Background

Identification through fingerprints is a major tool in law enforcement. In order to make a positive identification of a suspect, that subject's fingerprint must be on-file for comparison to the imprints left at a crime scene. The digital storage of each individual fingerprint requires about 9.8 million bytes of data, resulting in approximately 245 trillion bytes for storage of all the fingerprint cards on-file at the FBI (15). This number can be lowered by compressing the fingerprint image in preparation for storage.

Image compression, which reduces the data storage requirement, is a three-stage process: invertible transformation; quantization; and redundancy removal (31). The transformation stage, where the image coefficients are translated to a new coordinate system, is the most important component of the algorithm (31). Although the transformation algorithm requires complex mathematics to implement, its benefits are numerous, especially when the algorithm is accomplished in real-time. This literature review discusses four transformation techniques and a novel real-time implementation.

2.2 Transformation Techniques

2.2.1 Fourier Methods. Traditional methods for transformation are based on the Fourier transformation process. The Fourier kernel, equation 2, an exponential, is the basis set for the traditional methods.

$$e^{-j2\pi(f_x x + f_y y)} \quad (2)$$

Two techniques which are used in image processing are distinguished by the segmentation of the image and processing on that segment. The standard transformation

technique for picture compression, established by the Joint Photographic Experts Group (JPEG), is a discrete cosine transform on 8 X 8 pixel blocks (31). JPEG is an effective means of compressing image data and is considered the "application to beat in most applications" (31). An alternative to JPEG is the Localized Cosine Transform (LCT). Developed in an attempt to solve the blockiness problem of JPEG, the LCT technique has overlapping segments of bell-shaped functions instead of the discrete rectangle-shaped functions associated with JPEG (31).

2.2.2 Wavelet Methods. A more recent development, the wavelet transformation uses a different basis set for its transformation, the wavelet basis. Several wavelet functions have been developed (29). Because there are several basis functions for the wavelet transformation, one key advantage of this method over traditional Fourier methods is the flexibility in the basis selection. The Orthogonal Wavelet Basis (OWB) is distinguishable from the Best-Basis Wavelet (BBW) in that the Best-Basis algorithm bases its selection for the basis function on performance. The BBW compares several transformation outputs. The OWB is a simpler algorithm which uses only one basis for its algorithm (31).

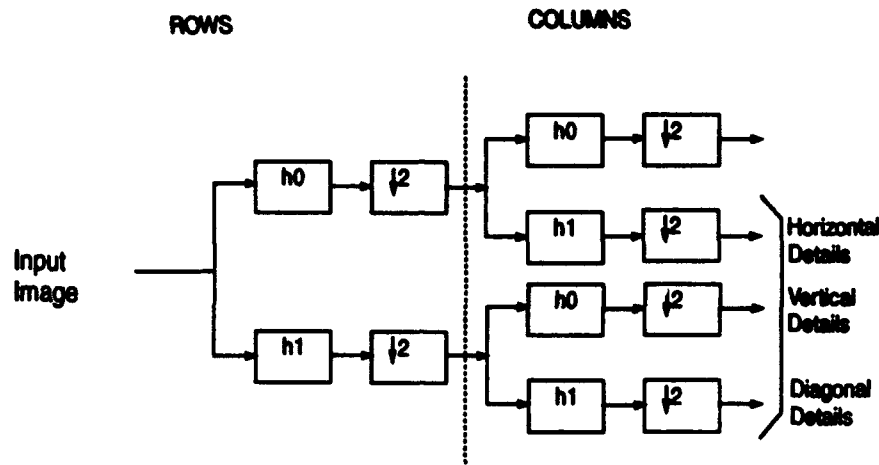


Figure 1. Two Dimensional Decomposition Algorithm (1).

For simplicity and speed, a multiresolution analysis (MRA) scheme was developed by Mallat for computing the wavelet transform coefficients at dyadic values of the scale and shift variables (23). The MRA is a sub-band coding scheme using a quadrature mirror filter bank for analysis and perfect reconstruction, where each level of decomposition filters the input image with a dyadically scaled wavelet. Figure 1 represents one stage of the multiscale decomposition algorithm, where the wavelet coefficients are captured in the horizontal, vertical, and diagonal detail images at each resolution level (1). In the flow diagram in figure 1, the input image is fed to two separate filters, h_0 and h_1 , which are effectively low pass and band(high) pass filters respectively. Notice that in the decomposition algorithm each channel is downsampled by the dyadic value which maintains the proper shift and scaling operation for the next level of decomposition. The filter operation is accomplished in both dimensions, rows and columns, creating four filtered versions of the original input. The three channels labeled details in figure 1 are stored as the wavelet transform coefficients, with the fourth channel returned to the input stage for the next level of decomposition.

Each level of decomposition scales the filters, resulting in coarser approximation and detail coefficients. In equations 3 and 4, the scaling and wavelet functions, ϕ and ψ , are scaled by the variable m which corresponds to a level of decomposition. The first level of decomposition is considered the $m = 0$ level of decomposition, with each successive level represented by $m = 1, 2, \dots$.

$$2^{-m/2}\phi(2^{-m}t - n) \quad (3)$$

$$2^{-m/2}\psi(2^{-m}t - n) \quad (4)$$

2.2.3 Analytical Comparison. The wavelet transformation has advantages over the traditional Fourier based techniques. It is capable of representing the image at several scales in a redundant manner, due to the multi-scale property of the wavelet transformation (27). This capability is useful for extracting characteristics of a fingerprint image. The wavelet transform displays larger scale characteristics, such as the fingerprint ridges, as well as smaller scale characteristics, such as the position and shape of the pores. It is important to access both levels of detail (16). Since prints from a crime scene are usually less than perfect, investigators must extract as much information as possible from the available print to match with existing prints from a data base. The wavelet transform can also specify exact location of frequency spectrum. The localization of the image in both time and frequency makes the wavelet transformation more efficient for analysis of digital images (29).

2.2.4 Experimental Comparison. The FBI directed a study which compared four transformation methods for compressing fingerprint images: JPEG; LCT; OWB; and BBW (31, 15). According to the FBI, there are two potential users of the compressed fingerprint image: automatic recognition algorithms and human experts. These users' analyses of the compressed image established the comparison basis for

the transformation methods. When read by the recognition algorithms, the compressed image is expected to contain the same minutiae relationships as the original image. Additionally, the compressed image should stand up to expert review for detail (15, 16).

The wavelet transformation outperformed the Fourier methods in both areas of comparison. The compressed images were fed into the Home Office Matcher, an algorithm employed by the FBI for matching suspect fingerprint images to stored ones. Images compressed by the wavelet transformation resulted in an increased number of correctly detected aspects compared to the original images, while the images compressed by the JPEG and LCT transformations resulted in a reduction in detected aspects (15). The wavelet compressed images also stood up better to close inspection by fingerprint experts. When the compressed images were brought under close inspection, the images compressed by the wavelet transform showed minimal distortion at 20:1 compression ratio, while images compressed by the Fourier techniques showed excessive distortion at that same compression ratio (16). Overall, the wavelet transformations performed considerably better than the Fourier-based techniques when the compression ratio exceeded 10:1 (31, 16).

2.2.5 Symmetric Wavelet Transform. The standard for fingerprint compression adopted by the FBI involves a symmetric wavelet transformation (4). The symmetric wavelet transform takes advantage of symmetric extension of the finite input signal (fingerprint image), accounting for the boundary conditions in a manner which eliminates the jump discontinuity introduced by a periodic extension (5). A symmetric extension has advantage over periodic extension in terms of compressibility.

In image coding, quantization errors will often be most prominent around the edges in the images; it is a property of our visual system that we are more tolerant of symmetric errors than asymmetric ones. In other words, less asymmetry would result in greater compressibility for the

same perceptual error. Moreover, symmetric filters make it easier to deal with the boundaries of the image (17).

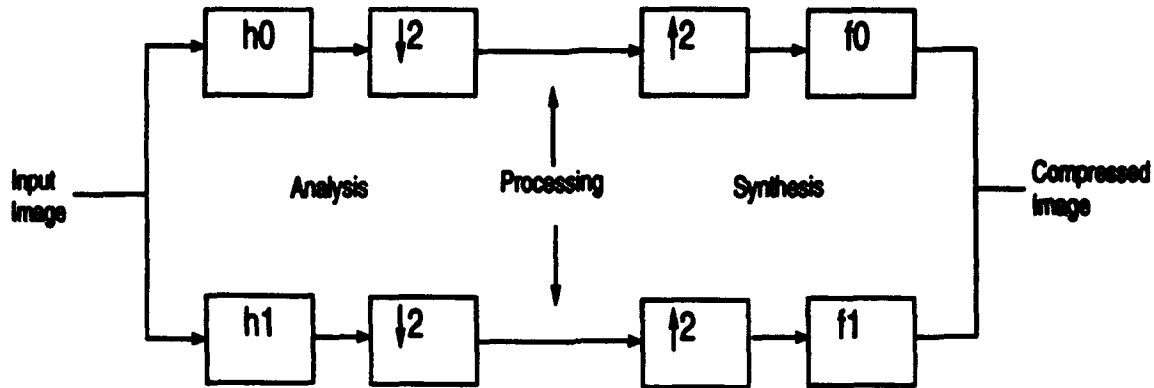


Figure 2. One Dimensional Two-Channel Subband Coder

The decomposition of a signal into wavelet coefficients can be compared to a Quadrature Mirror Filter (QMF) in structure. In order to use symmetrical filters and maintain linear phase, it is necessary that the analysis filters differ from the synthesis filters (9). An input image is decomposed using the filters h_0 and h_1 (see figure 2), fed to a signal processing algorithm (i.e. image compression through vector quantization), and recreated using a different set of filters, f_0 and f_1 . The coefficients for the synthesis filters are generated from the analysis filter coefficients. The filter coefficients for f_0 and f_1 are related to the analysis filters h_0 and h_1 by the following relationships:

$$h_{1n} = (-1)^{n+1} f_{0-n+1}$$

$$f_{1n} = (-1)^{n+1} h_{0-n+1}$$

In this manner, the filter bank maintains linear phase and symmetry.

Thus the wavelet transform is more effective at compressing fingerprint data than traditional Fourier methods, displaying improvement in both distortion analysis and recognition. The same symmetric biorthogonal wavelet transform could be applied to the fingerprint for image analysis, enhancing the identification process. The technologies involved in implementing the optical biorthogonal wavelet transform are discussed in the next chapter. The wavelet transform is then applied to an optical fingerprint identifier.

III. Methodology

This research combines two holographic techniques for optical fingerprint identification. This Chapter describes the methods used to construct and implement the holograms. First, the biorthogonal wavelet filter used by the FBI for image compression is constructed. The wavelet filter is the Fourier spectrum representation of the wavelet function. The wavelet filter was created using a binary, detour phase technique. The wavelet transform was realized with continuous shift variables through an optical correlation between the input image and the wavelet filter. A telescopic lens arrangement adjusted the scale variable of the wavelet transform continuously. The second hologram was used as a matched spatial filter (MSF) created using the Vander Lugt method with a reference beam and a thermoplastic film plate.

3.1 Wavelet Filter

The wavelet transform is simply a correlation between the input image and the wavelet function (Equation 1). Optics implements the wavelet transform in real-time with continuous shift variables using optical correlation. A collimated laser illuminates the input image, the beam is passed through a positive lens, a representation of the wavelet filter is positioned in the back focal plane of the positive lens, and the resulting image is passed through a second lens resulting in the wavelet transformed image. This arrangement is shown in Figure 3.

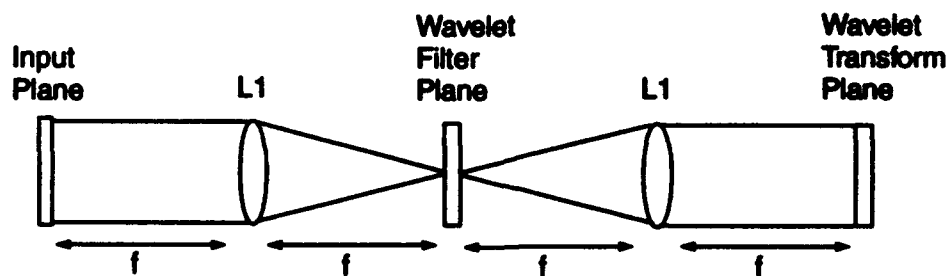


Figure 3. Diagram of Optical Correlator

The wavelet filter was a computer generated hologram, representing the Fourier transform of the wavelet function. This complex mathematical representation was constructed from the finite impulse response (FIR) coefficients for the wavelet.

3.1.1 Mathematical Development of Wavelet and Basis Filters. This research implemented the same wavelet function chosen by the FBI for image compression. The symmetric FIR filters used in the creation of the biorthogonal wavelet filter were chosen because of their demonstrated ability to compress FBI fingerprint images (31, 15). The values for the nine/seven tap symmetric filter coefficients used in this research are given by Table 1.

Tap	Exact Value	Approximate Value
$h0_0$	$-5\sqrt{2} x_1(48 x_2 ^2 - 16Rx_2 + 3)/32$	+0.85269867900940
$h0_{\pm 1}$	$-5\sqrt{2} x_1(8 x_2 ^2 - Rx_2 + 3)/8$	+0.37740285561265
$h0_{\pm 2}$	$-5\sqrt{2} x_1(4 x_2 ^2 + 4Rx_2 - 1)/16$	-0.11062440441842
$h0_{\pm 3}$	$-5\sqrt{2} x_1(Rx_2)/8$	-0.023849465019380
$h0_{\pm 4}$	$-5\sqrt{2} x_1/64$	+0.037828455506995
$h1_{-1}$	$\sqrt{2} (6x_1 - 1)/16x_1$	+0.78848561640566
$h1_{-2,0}$	$-\sqrt{2} (16x_1 - 1)/64x_1$	-0.41809227322221
$h1_{-3,1}$	$\sqrt{2} (2x_1 + 1)/32x_1$	-0.040689417609558
$h1_{-4,2}$	$-\sqrt{2} /64x_1$	+0.064538882628938

Table 1. Analysis Wavelet Filter Coefficients (5).

where (6):

$$\begin{aligned}
 x_1 &= A + B - \frac{1}{6} \\
 x_2 &= -\frac{(A+B)}{2} - \frac{1}{6} + i\sqrt{3}\frac{(A-B)}{2} \\
 A &= \sqrt{\frac{-14\sqrt{15} + 63}{1080\sqrt{15}}} \\
 B &= \sqrt{\frac{-14\sqrt{15} - 63}{1080\sqrt{15}}}
 \end{aligned}$$

The equations 5-8 demonstrate how to generate the frequency domain representation of each of the filters. First, the transfer functions for each of the filters were generated from their impulse response.

$$m_0(\hat{x}) = \frac{1}{\sqrt{2}} \sum_n h_{0n} e^{-in\hat{x}} \quad (5)$$

$$m_1(\hat{x}) = \frac{1}{\sqrt{2}} \sum_n h_{1n} e^{-in\hat{x}} \quad (6)$$

The basis function in the frequency domain for the analysis filter was determined by equation 7.

$$\phi(\hat{x}) = \frac{1}{\sqrt{2\pi}} \prod_{j=1}^{\infty} m_0(2^{-j}\hat{x}) \quad (7)$$

The transform of the wavelet function for the analysis filter was determined by the product of the transfer function for the synthesis filter and the transformed basis function evaluated at half the frequency as shown in equation 8.

$$\psi(\hat{x}) = m_1\left(\frac{\hat{x}}{2}\right)\phi\left(\frac{\hat{x}}{2}\right) \quad (8)$$

The filter h_0 in Figures 1 and 2 was represented by the basis function in equation 7. The time and frequency domain representation for the basis function are shown in Figure 4. Notice the low pass characteristic of the basis filter $\phi(\hat{x})$ which

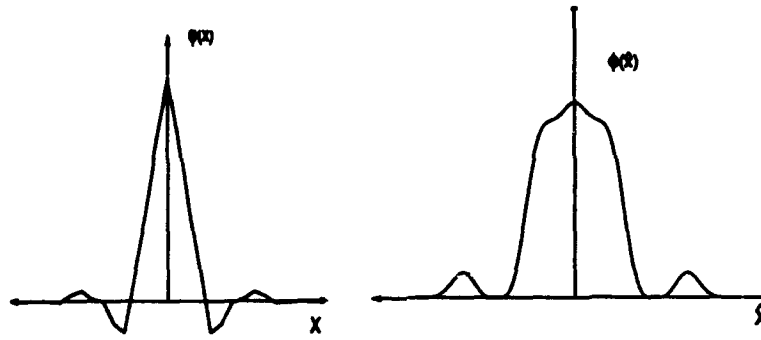


Figure 4. Basis function $\phi(x)$ and its Fourier spectrum $\phi(\hat{x})$

is both real and symmetric. The filter h_1 in Figures 1 and 2 was represented by the wavelet function in equation 8. The time and frequency domain representation for the wavelet function are shown in Figure 5. The wavelet filter $\psi(\hat{x})$ was a bandpass

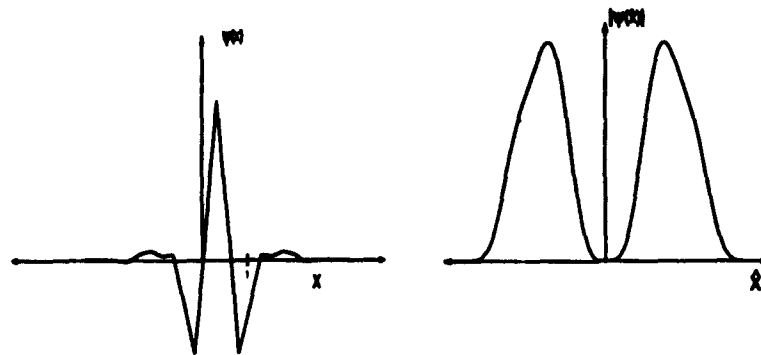


Figure 5. Wavelet function $\psi(x)$ and the magnitude of its Fourier spectrum $\psi(\hat{x})$

filter, possessing both symmetry and linear phase. The wavelet function exhibits compact support, a favorable aspect for localizing image spectrum content. This condition was beneficial for reducing aliasing effects brought on by sampling of the wavelet filter, discussed in the section on binary detour phase holograms.

3.1.2 Binary Detour Phase Hologram. Representing the complex-valued wavelet filter on an intensity-only medium (such as a photographic plate) required holography. A binary, detour phase hologram represented both the magnitude and phase of the complex function at discrete sample intervals (7). The first consideration when constructing the hologram was the extent of the original time domain function. According to sampling theory, the wavelet filter must be sampled at small enough intervals in order to prevent aliasing. The sample interval must not exceed the reciprocal of the wavelet function's extent. In this manner, the compact support of the wavelet filter helped avoid this problem, since the wavelet function had limited extent. The detour phase hologram was divided into an array of equal dimensional cells. Each of the opaque cells corresponded to a sample point in the complex function plane. Within each of these cells was placed a rectangular aperture. The magnitude and phase of the sample point defined the size and position of the aperture within the cell. Figure 6 shows the layout for one cell.

The magnitude of the sample point defined the height of the rectangle: $h_{nm} = A_{nm}d_y$. The rectangle was centered vertically within the cell and each step in magnitude, A_{nm} , equated to subsequent increase in the height of the rectangle. The magnitude values of the complex function were scaled (normalized) so that the maximum extent of the function corresponded to the largest extent of the cell. The width of each rectangle, w , was kept constant. The value of the width determined the efficiency of the hologram. A wider value allowed more light to pass through the hologram, which was an important factor in this experiment. However, there was a trade-off between hologram efficiency and distortion due to phase quantization. The position of the rectangular aperture was determined by the phase of the sample

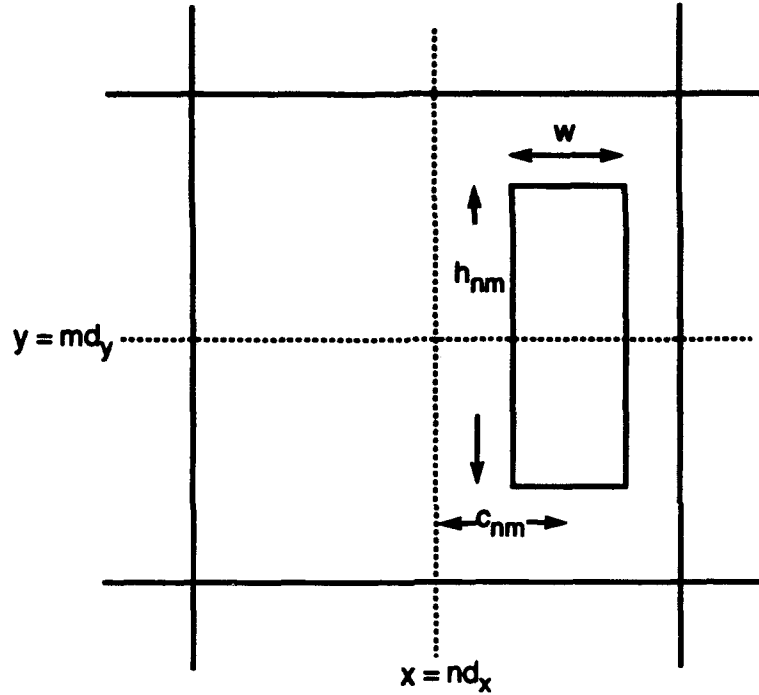


Figure 6. Sample Cell of Detour Phase Hologram (30).

point, $c_{nm} = \frac{\phi_{nm}}{2\pi}$. Centering the aperture equated to zero phase, shifting to the right side of the cell was $+\pi$ phase, and shifting the rectangle to the far left of the cell was $-\pi$ phase. The number of quantization levels for the phase was determined by the ratio of the cell width to the rectangle width. This was a major consideration since the primary cause of distortion of the original image by this holographic technique lay in the sampling of the phase (32). The higher the number of levels the lower the distortion caused by the sampling of the phase. This effect was best illustrated by the relative intensity value of the m th order false image to the zero order image:

$$(mN + 1)^{-2} \quad (9)$$

The value, N , in equation 9 was the number of quantization levels. Increasing N diminished the intensity of the false images, and limited the distortion. The holograms for this research were created using a laser printer. The negative image was

transcribed onto a transparency to be used to create a photo-reduced glass slide. The laser printer was limited to a 400 dots-per-inch resolution, so for an 8 inch transparency, 3200 points was the upper limit for each dimension. The holograms had a total of 161 sample points in each dimension, with each cell made up of 16 X 16 pixel points. The 161 sample points was well within the limit set by sampling theory. With these dimensions, the hologram was made up of a total of 2576 points across each of the dimensions. Because the actual resolution of the laser printer fell short of the 3200 point limit, this value seemed appropriate. The width of each rectangle was chosen to be 8, half the width of the cell, for a 50 percent duty cycle. This width assured that the hologram would pass a sufficient amount of light and still allow for 9 distinct horizontal positions for the rectangle within each of the cells. Nine levels of phase quantization limited the distortion according to equation 9. The relative intensity for the first order false image was one one-hundredth that of the original. A mathematical analysis of the array of cells helped to understand how the size and position of these rectangles represented magnitude and phase of a complex function. In equation 10, the function $t_1(x, y)$ represented the hologram, which was simply an array of rectangular apertures. For this analysis, the Fourier transform of the array of rectangles was calculated and represented by the function $T_1(u, v)$. This function was rewritten as a summation over the array dimensions n and m as shown, which is the discrete Fourier transform of the original function.

$$\begin{aligned} T_1(u, v) &= \iint_{-\infty}^{\infty} t_1(x, y) e^{-j2\pi(ux+vy)} dx dy \\ &= \sum_n \sum_m G_{nm}(u, v) e^{-j2\pi(nd_x u + md_y v)} \end{aligned} \quad (10)$$

The function G_{nm} was the Fourier transform of the rectangle functions. Each Sinc function had widths defined by the values h_{nm} and w , the height and width of the rectangle. The phase factor in equation 11 was due to the shift value for each

rectangle within the cell, c_{nm} .

$$G_{nm}(u, v) = \frac{\sin \pi w u}{\pi u} \frac{\sin \pi h_{nm} v}{\pi v} e^{-j2\pi c_{nm} u} \quad (11)$$

A sample point equating to the center of the arrays was chosen for this example. This value was substituted into the equation. The power series expansion for the Sinc function was evaluated and approximated as shown.

$$\begin{aligned} u_c &= \frac{k}{d_x} \\ v_c &= 0 \end{aligned}$$

$$G_{nm}(u, v) = \frac{\sin \pi w u}{\pi u} h_{nm} e^{-j2\pi k c_{nm}/d_x} \times (1 + \pi v h_{nm}^2/6 - j2\pi c_{nm}(u - u_c)) + \dots \quad (12)$$

This value was substituted back into equation 10.

$$T_1(u, v) = \frac{\sin \pi w u}{\pi u} \sum_n \sum_m (1 + Q_{nm}) h_{nm} e^{-j2\pi k c_{nm}/d_x} \times e^{-j2\pi (n d_x u + m d_y v)} \quad (13)$$

The values for the height and shift were substituted back into the equation 13: $h_{nm} = A_{nm} d_y$ and $c_{nm} = \frac{\phi_{nm}}{2\pi} d_x$. What was left in equation 14 was the discrete Fourier transform of the original sample point of magnitude A_{nm} and phase ϕ_{nm} . The additional factor Q_{nm} was due to phase distortion. This analysis showed that the array of rectangles did indeed represent the original complex function.

$$T_1(u, v) = \frac{\sin \pi w u}{\pi u} \sum_n \sum_m (1 + Q_{nm}) d_y A_{nm} e^{-jk\phi_{nm}} \times e^{-j2\pi (n d_x u + m d_y v)} \quad (14)$$

The hologram transparency was created using the program in the appendix. The finished product was a series of opaque rectangles representing the negative of the hologram, see Figure 7. This transparency was used to create a photo-reduced glass slide for use on an optics bench. For reducing the transparency, the negative was taken to the Cooperative Electronics Materials Process Lab at Wright Patterson

AFB for reduction onto a high resolution glass plate. The Dekacon optical system used for reduction of the CGH is shown in Figure 8.

3.1.3 Two Dimensional Filters. As shown in Figure 1, the decomposition of a two dimensional signal using wavelet analysis resulted in combinations of the wavelet and basis filters. For this research there were three filters required to capture the vertical, horizontal, and diagonal details of the image. These three frequency channels stemmed from the combination of filtering operations across the rows and columns of the input image. In this manner, combination of the transforms of the wavelet function and the basis function resulted in horizontal (Figure 9), vertical (Figure 10), and diagonal (Figure 11) wavelet filters. Three different filters were used in the optical experiment: the horizontal, vertical, and diagonal filter. The filters were created by combination of the basis and wavelet function depicted in equations 7 and 8 respectively.

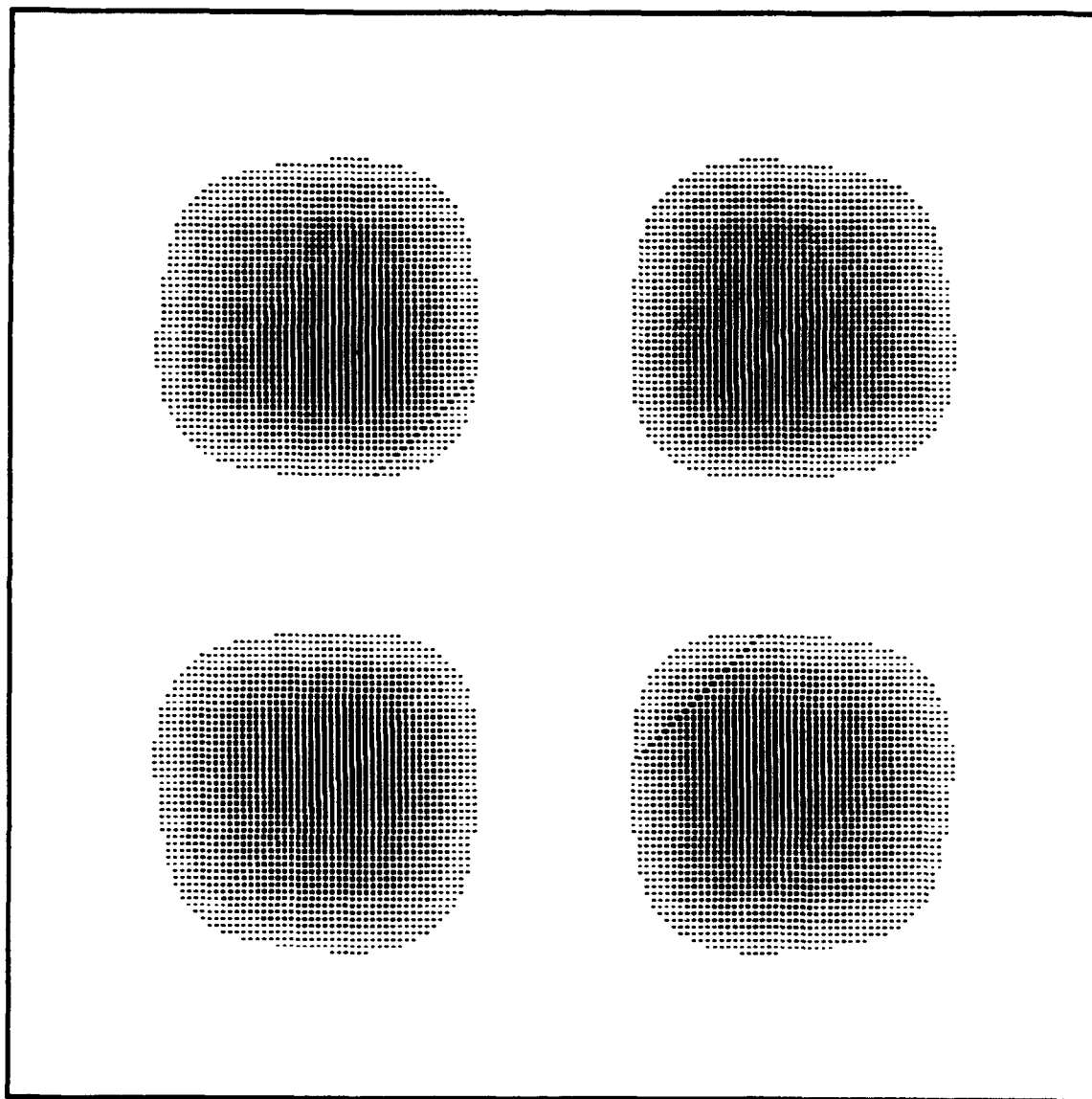


Figure 7. Transparency of Detour Phase Hologram

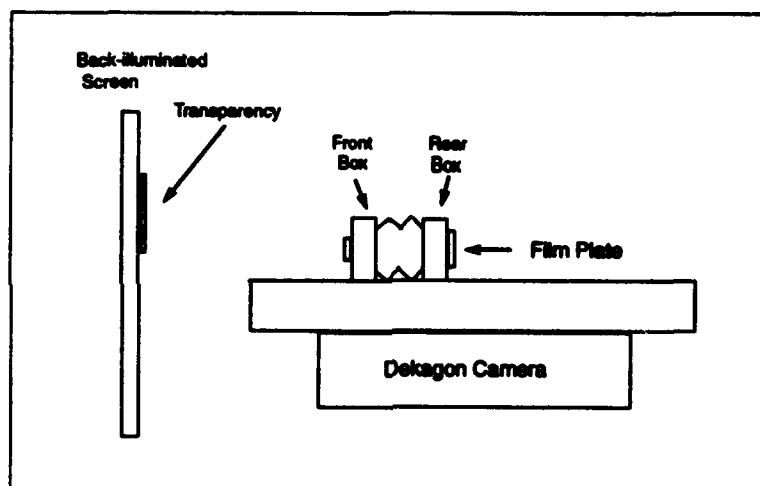


Figure 8. Dekacon Camera System

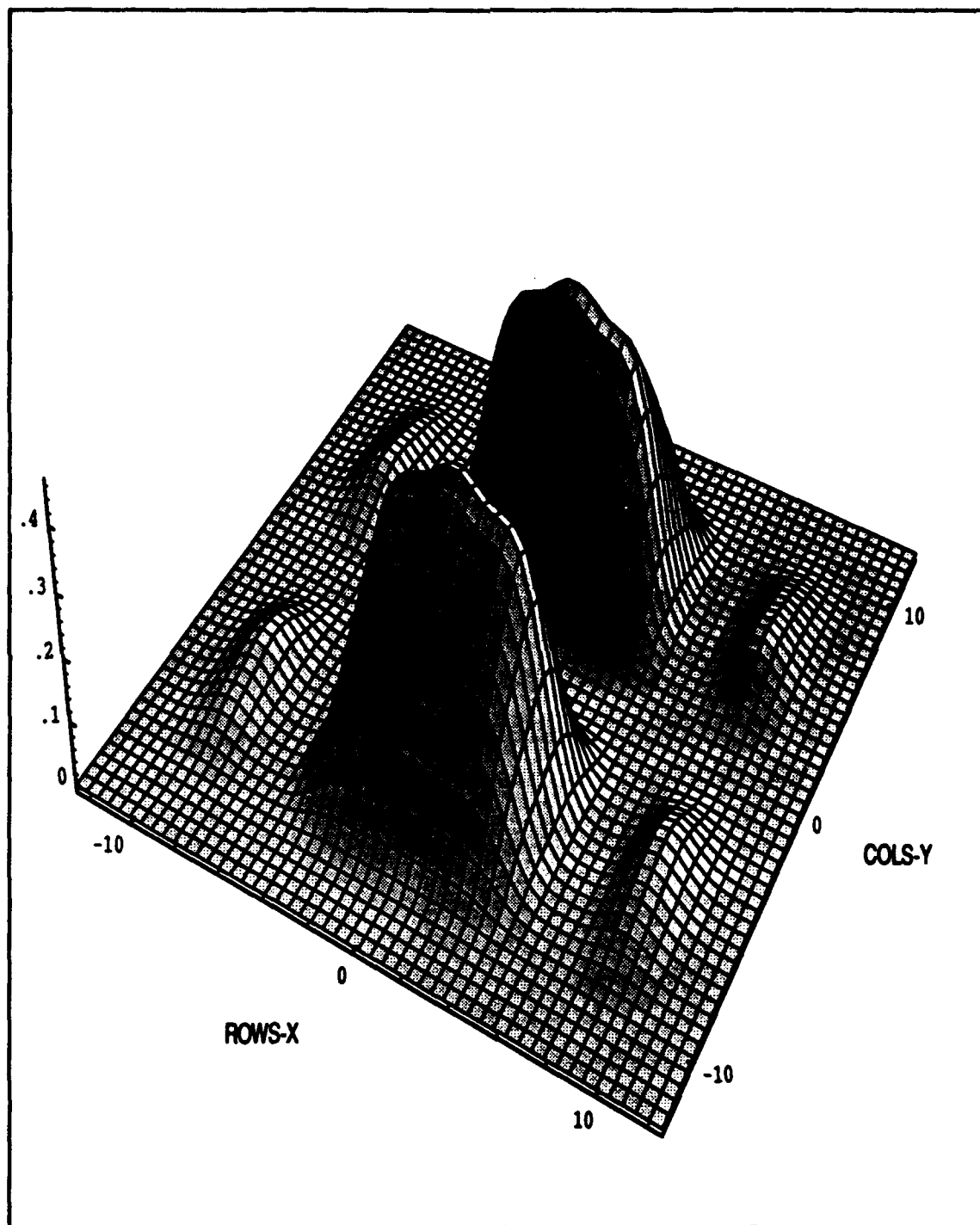


Figure 9. Horizontal Wavelet Filter: $\phi(\hat{x})\psi(\hat{y})$

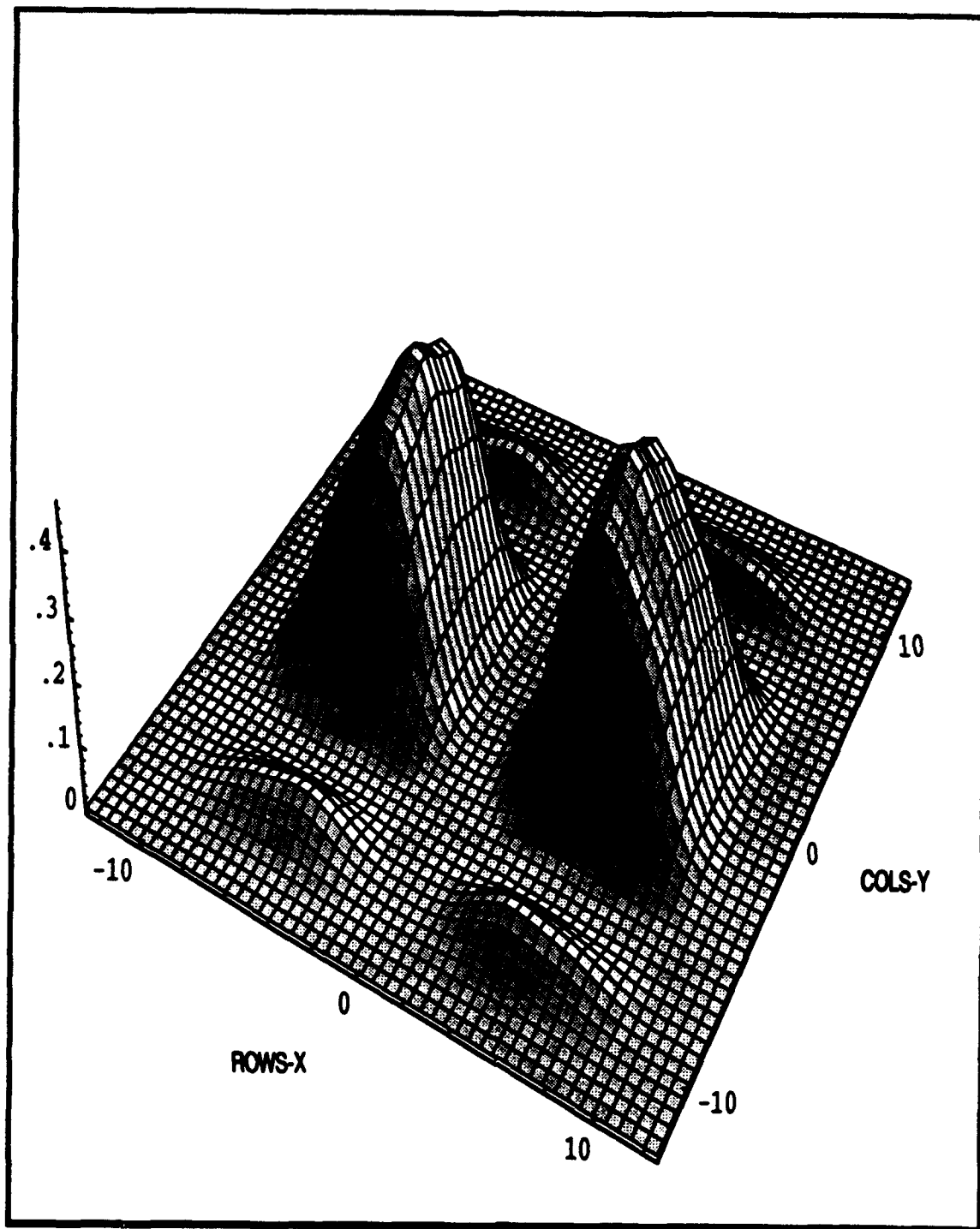


Figure 10. Vertical Wavelet Filter: $\psi(\hat{x})\phi(\hat{y})$

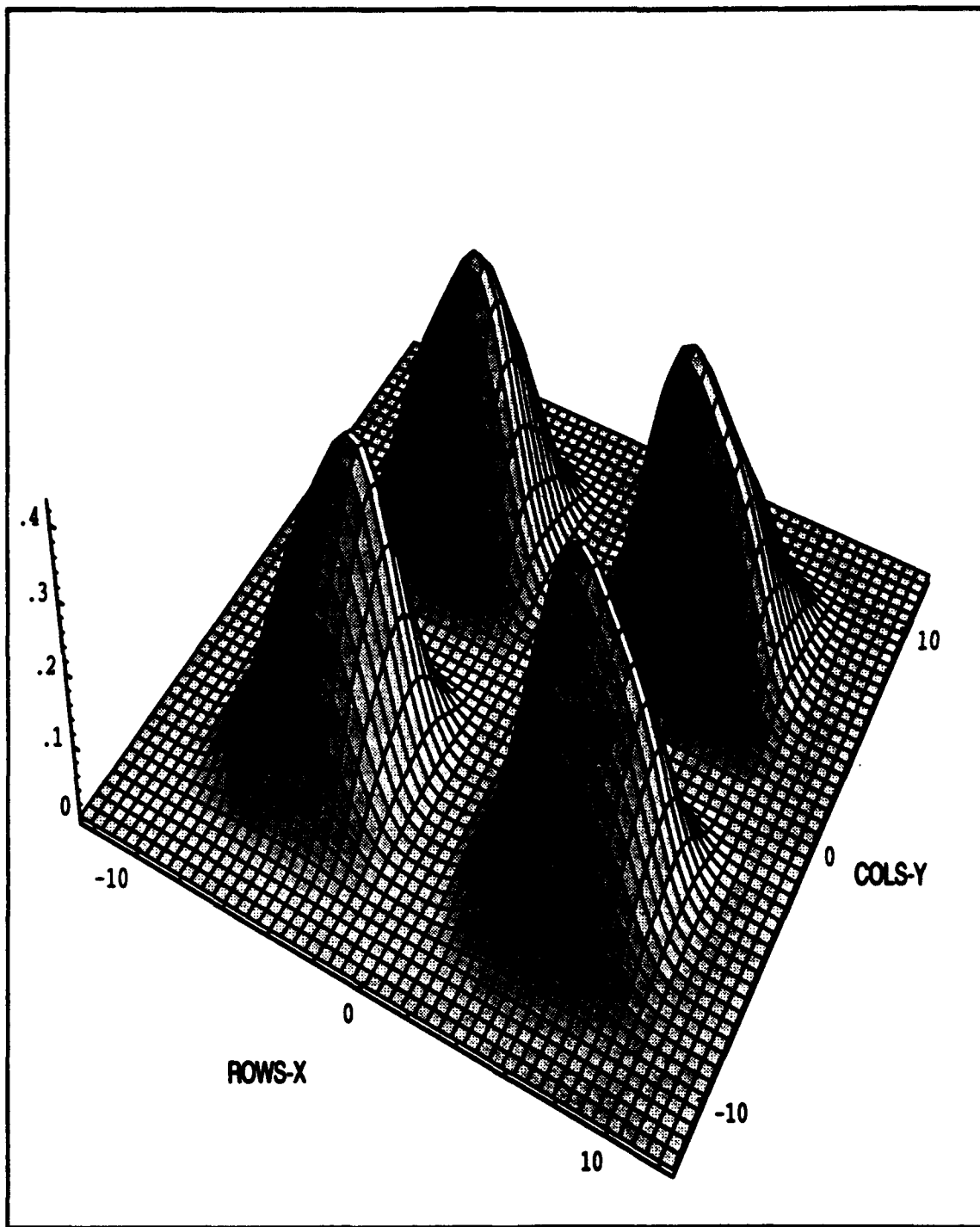


Figure 11. Diagonal Wavelet Filter: $\psi(\hat{x})\psi(\hat{y})$

3.2 Optical Architecture

In order to first characterize the optical wavelet transform, a MOSLM was used to present images for study. The optical arrangement was developed to be an improvement on the MRA algorithm. The MRA algorithm decomposed the input signal into its wavelet coefficients at dyadic values for the shift and scale variable, necessary for swift calculation of the wavelet transform. Because the wavelet transform was simply a correlation between the input image and the wavelet function, optics implemented the wavelet transform in real-time with continuous distribution of the shift variable. This was an advantage over the MRA algorithm. Using a variation of the optical correlator allowed continuous distribution of the scaling function as well.

Continuous distribution of the scaling function was realized with the configuration depicted in Figure 12. This was an improvement over the optical correlator in Figure 3 because the negative lens, L2, added flexibility over the scaling of the wavelet filter. In the configuration in Figure 12, a binarized image was introduced in

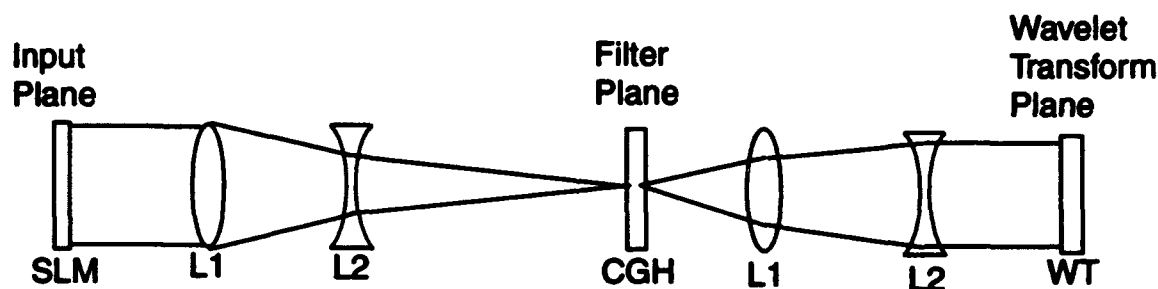


Figure 12. Adjustable Scale Optical Correlator

the input plane on a MOSLM. Using a telescopic lens arrangement to perform the Fourier transforming stages in the optical correlator allowed variation of the scaling of the Fourier transform. This arrangement has been effective in developing small scale optical correlators and can now be used for scaling the wavelet filter (3). The positive lens, L1, was placed a focal length away from the input plane. The Fourier

transform of the image appeared at the back focal plane of lens L1. Lens L2 imaged the transformed image onto the filter plane, where the transform was a virtual object to lens L2. As long as the transformed image fell within the focal length of L2, a magnified real image was created at the filter plane. The placement of L2 relative to the back focal plane of L1 and the subsequent placement of the wavelet filter determined the scaling of the transform onto the wavelet filter. The same process was duplicated in the scaling of the wavelet transform onto the camera which captured the wavelet transform plane. To determine the minimum scaling of the wavelet filter, the system was analyzed according to the dimensions of the MOSLM and the wavelet filter.

The minimum focal length for the transforming lens in a matched spatial filter is determined by the spacing of the input image pixels (d_1), the spacing of the filter plane pixels (d_2), the dimension of the filter (in pixels) (N_2), and the wavelength of the laser source (λ) (11).

$$F = \frac{N_2 d_1 d_2}{\lambda} \quad (15)$$

With the MOSLM pixel spacing of 76 μm , the filter plane pixel spacings of 63 μm , the filter plane pixel dimension of 161 element array, and the wavelength of the laser at 632.8 nm; the minimum focal length was 1.22 meters. This focal length was the $m = 0$ or original wavelet for this experiment. Repositioning of lens L2 and the filter plane allowed a continuous variation of the scaling variable by expanding the Fourier transform onto the wavelet filter plane. In this arrangement, only one hologram for each of the wavelet filters was needed to produce multiple scale resolutions.

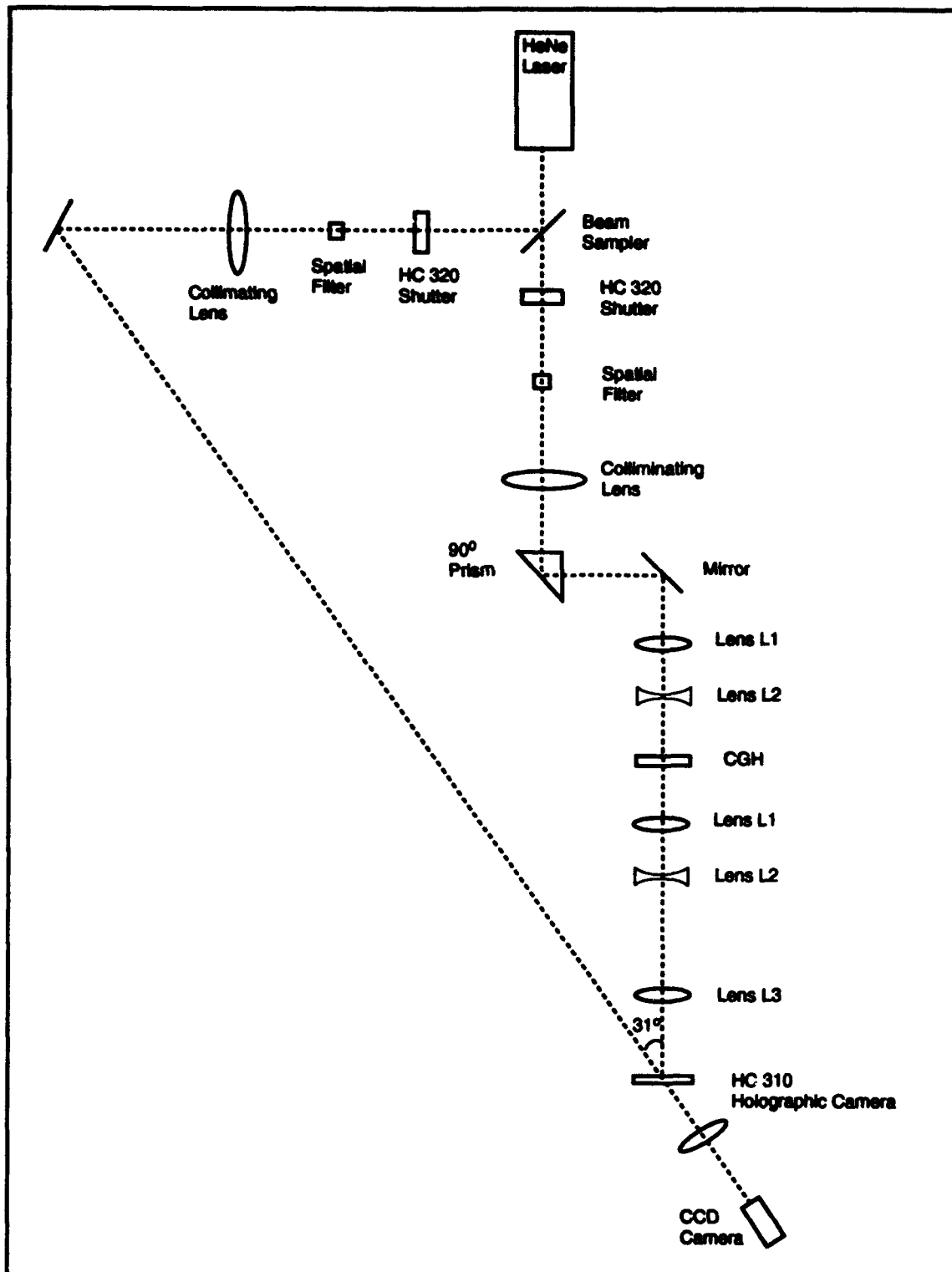


Figure 13. Improved Optical Wavelet Fingerprint Identification Arrangement

3.3 Optical Wavelet Fingerprint Identification

After the wavelet filter was characterized, it was used in an optical fingerprint identifier. The optics bench arrangement is shown in Figure 13. In this arrangement a fingerprint image was scanned into the system using a 90 degrees prism. By placing the person's finger onto the prism, the areas where the fingerprint ridges came in direct contact with the surface of the prism were areas where the laser beam was absorbed and not reflected into the system. Thus, the fingerprint image was read into the system using frustrated total internal reflectance.

The optical fingerprint identifier used a matched spatial filter (MSF) for discriminating between fingerprint images. In order to create the MSF, the second hologram was created using Vander Lugt filtering.

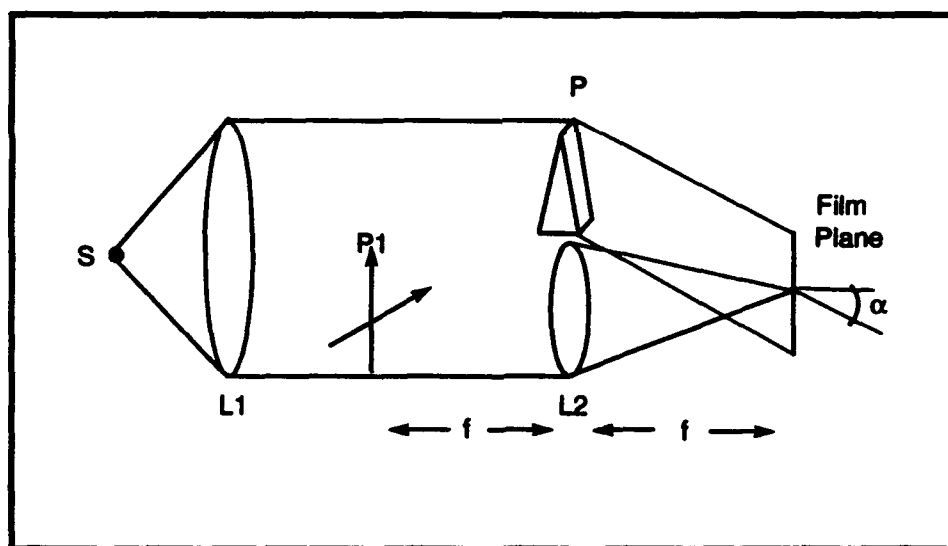


Figure 14. Vander Lugt Filter (18).

3.3.1 Vander Lugt Filter. The MSF was created through use of Vander-Lugt's method of interferometrically recorded frequency-plane masks (22). The optical arrangement is shown in Figure 14. The Fourier spectrum of the wavelet transformed fingerprint image was realized in the back focal plane of the lens, L3 in

Figure 13. A reference beam was split off from the laser beam and interfered with the spectral content of the wavelet transformed fingerprint image. In this manner the phase of the complex field was saved through the interference of the plane wave and the complex field. The resulting interference field was captured using a thermoplastic plate. The HC-300 Holographic recording camera was used to store the interference pattern of the Vander Lugt filter. The HC-300 developed the MSF electrically in about one minute. The thermoplastic plate was developed using a four step process shown in Figure 15. After the plate was developed, it was used as a MSF against which other wavelet transformed images could be compared. The fingerprint image was correlated with the wavelet filter, then the wavelet transform of the fingerprint was correlated with the MSF. The energy in the correlation peak captured in the diffracted beam off the hologram of the Vander Lugt filter was used to discriminate between fingerprints.

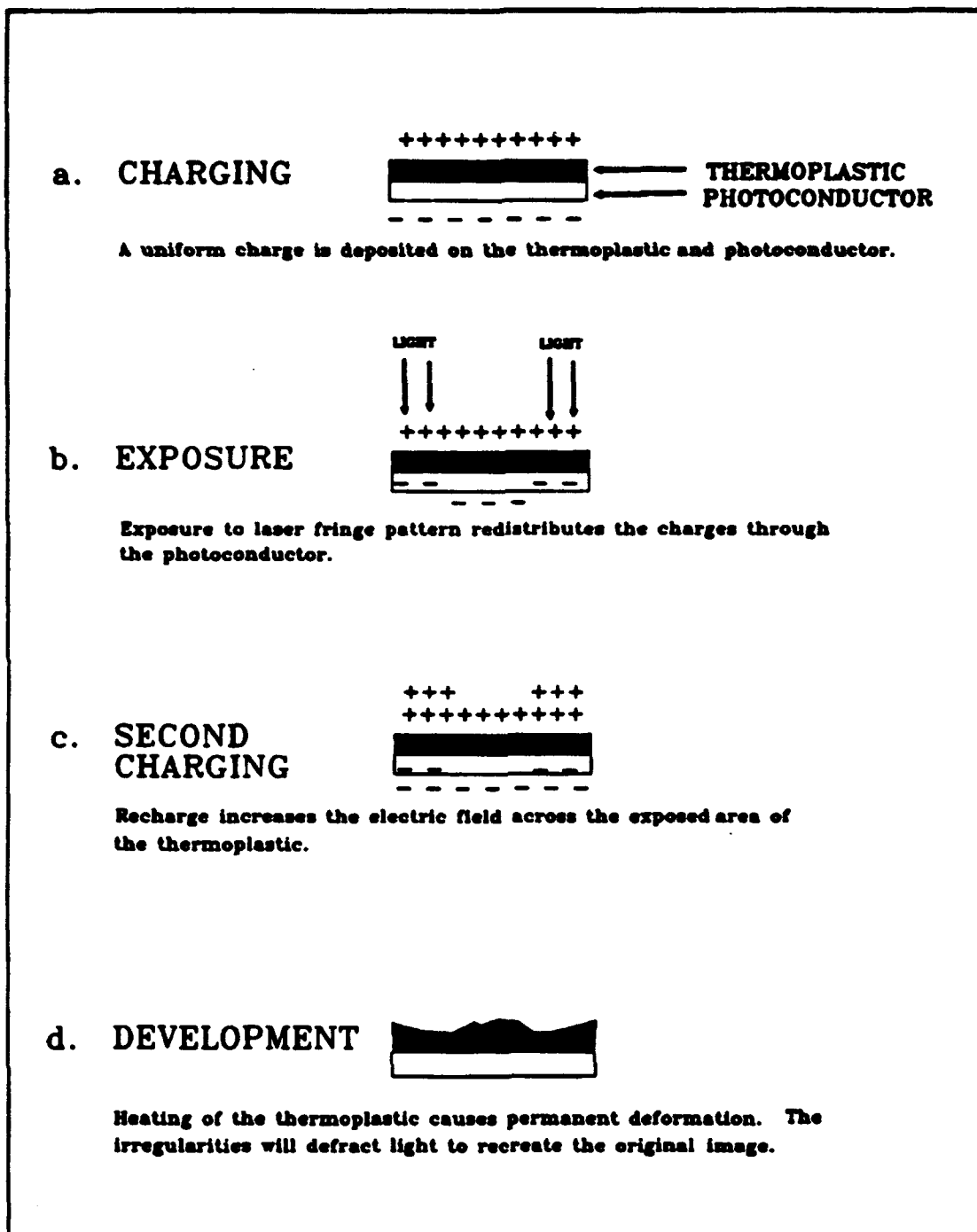


Figure 15. HC-500 Thermoplastic Recording Process (24).

IV. Results

This chapter presents and discusses the results based on the methodology described in Chapter III. The two topics of this research, application of an optical biorthogonal wavelet transform and development of an improved optical wavelet fingerprint identifier, are examined. Section 4.1 compares the optical biorthogonal wavelet transform to a digital wavelet transform of an image of the letter "E". Section 4.2 shows results from an optical biorthogonal wavelet transform of an image of "Lenna" and a fingerprint at three resolutions. The results from an improved optical wavelet fingerprint identifier are shown in Section 4.4. Finally, the rotational invariance of the improved wavelet optical fingerprint identifier are compared to the standard Vander Lugt matched filter method.

4.1 Characterization of Optical Biorthogonal Wavelet Transform

An image of the letter "E" was used in characterizing the optical process. The letter "E" was chosen because it contained easily recognized horizontal, vertical, and corner (diagonal) features. Three "types" of features were required to accurately characterize the set of three wavelet filters shown in Figures 9-11.

4.1.1 Input Image of Letter "E". The image of the letter "E" is shown in Figure 16. The original image was displayed on a MOSLM which had an array of 128 X 128 pixels. The image shown in Figure 16 was captured at the output of the optical correlator shown in figure 3 with the wavelet filter removed from the setup. Perfect alignment of the four lenses was assured by examining the output image shown here.

4.1.2 Horizontal Filter Results. The results from the horizontal filter are shown in Figures 17 through 20. The optical transform for the finest resolution horizontal wavelet filter is shown in Figure 17. This corresponds to level $m = 0$ in

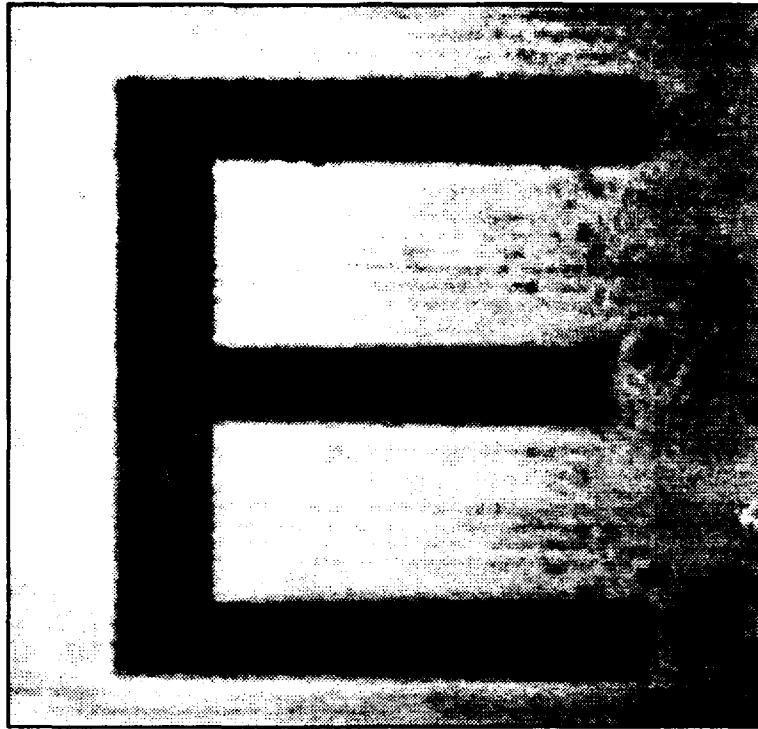


Figure 16. Capital Letter "E"

equations 3 and 4. The digitally produced transform for the same resolution wavelet filter is shown in figure 18. As shown in the figures, the horizontal structure of the image was emphasized by the horizontal filter. The horizontal details have been isolated from the rest of the image. The results from the optical process compared favorably with those created digitally.

The optical and digital results for the first dyadic scaling of the wavelet are displayed in Figures 19 and 20 respectively. As the wavelet function was doubled in size, its filter was diminished the same amount. The result was a filter which passed a lower band of spatial frequencies. Less horizontal structure was observed in the transformed image as expected. Again, the optical results were very similar to the digitally produced transform.

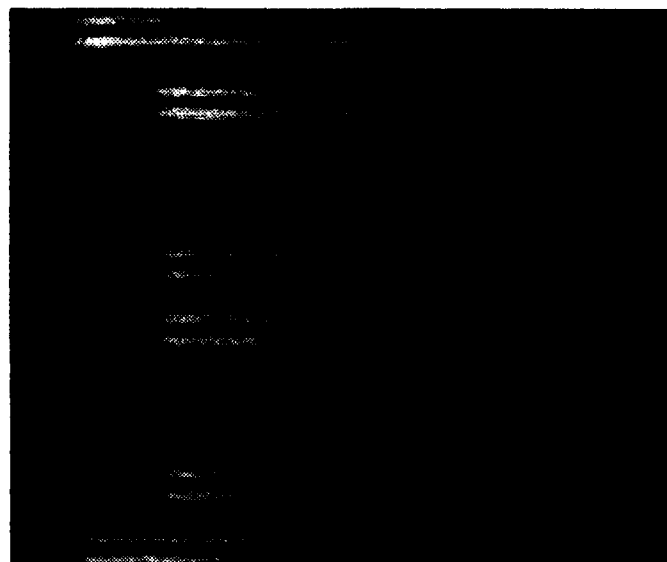


Figure 17. Optical Wavelet Transform for Horizontal Filter on Letter E, $m = 0$ Resolution

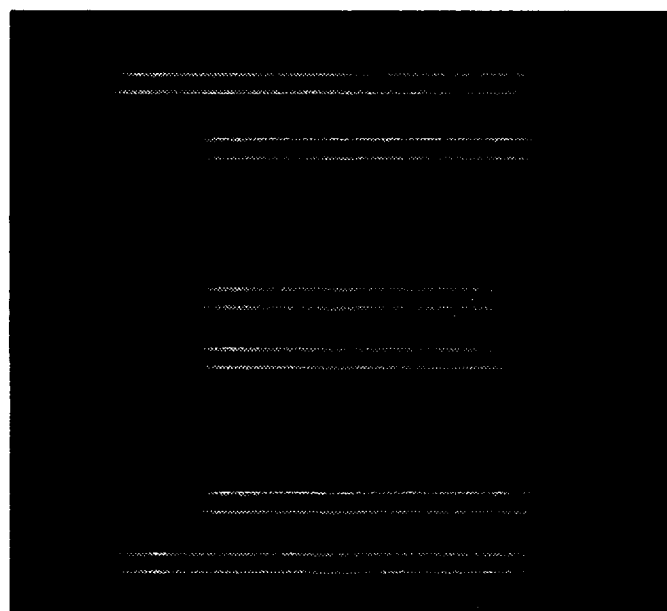


Figure 18. Digital Wavelet Transform for Horizontal Filter on Letter E, $m = 0$ Resolution

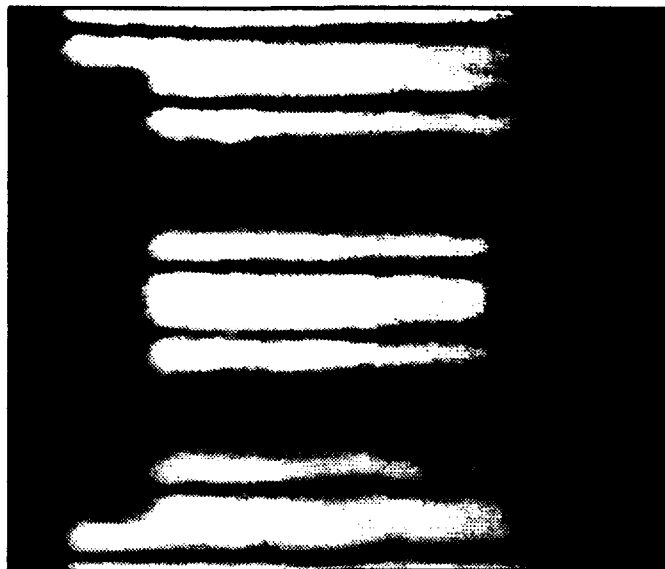


Figure 19. Optical Wavelet Transform for Horizontal Filter on Letter E, $m = 1$ Resolution

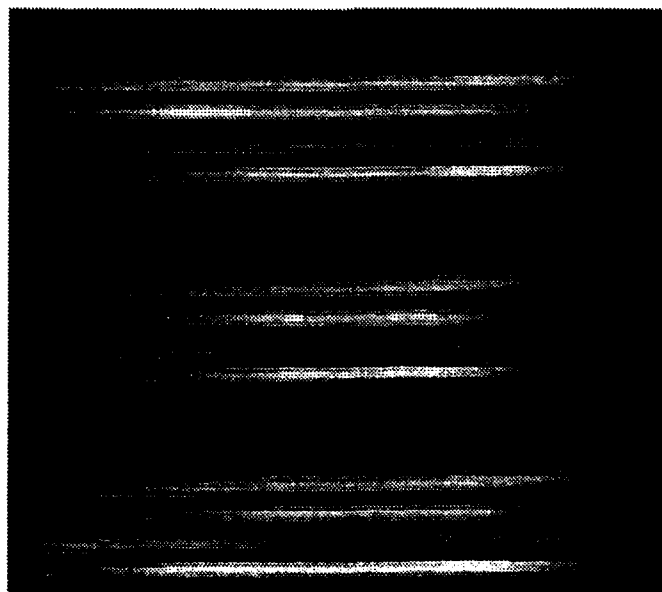


Figure 20. Digital Wavelet Transform for Horizontal Filter on Letter E, $m = 1$ Resolution

4.1.3 Vertical Filter Results. The optical transform for the finest resolution vertical wavelet filter is shown in Figure 17, and the digitally produced transform for the same wavelet filter is shown in Figure 18. The optical and digital results for the first dyadic scaling of the wavelet are displayed in Figures 23 and 24 respectively. The results from the optical process again compared favorably with those created digitally. In this case, the vertical details were isolated by the wavelet transform.

4.1.4 Diagonal Filter Results. The optical transform for the finest resolution diagonal wavelet filter is shown in Figure 25, and the digitally produced transform for the same wavelet filter is shown in figure 26. The optical and digital results for the first dyadic scaling of the wavelet are displayed on Figures 27 and 28 respectively. For the diagonal filter, the results from the optical process did not compare well with those of the digital ones. The images were faint and distorted in comparison to the other filters. This was due to the input image. Reviewing the image produced by the MOSLM in Figure 16, the corners of the letter were less than optimum. The MOSLM was old and missing some of the pixels in the array, making the image distorted. The lack of distinction in the corners reduced the amount of energy in those spatial frequencies which were passed by the diagonal wavelet filter. The limited intensity of the optical wavelet transform was due to this distortion in the input image.

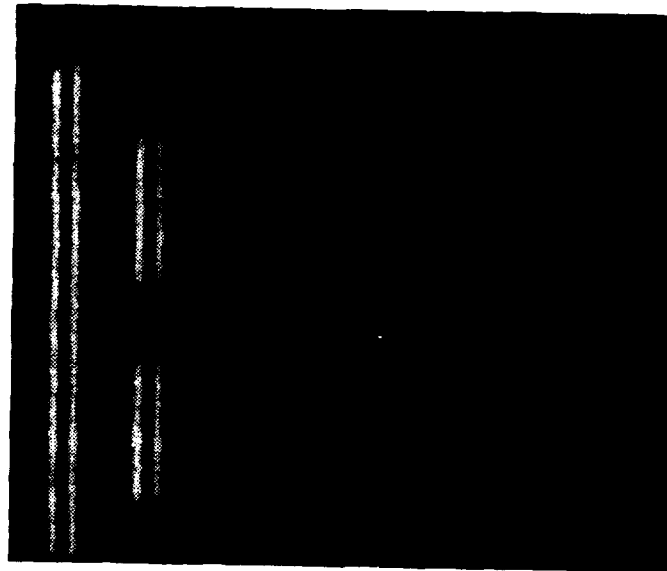


Figure 21. Optical Wavelet Transform for Vertical Filter on Letter E, $m = 0$ Resolution

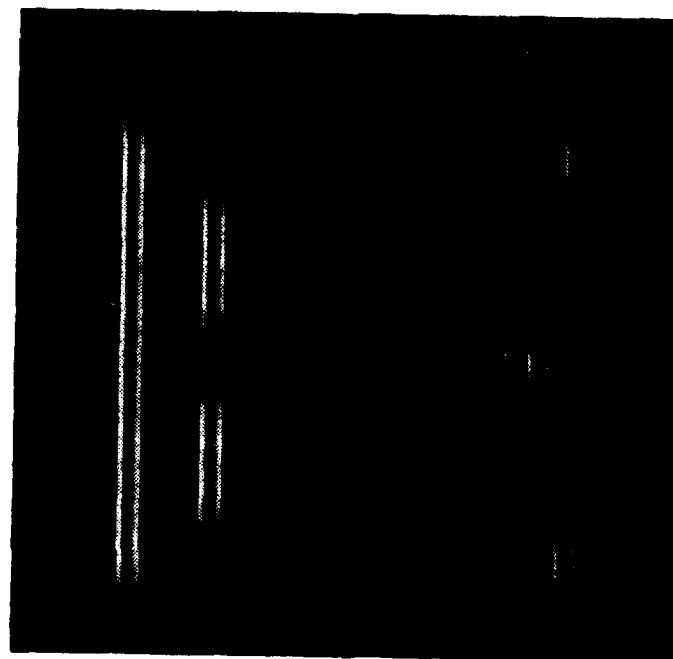


Figure 22. Digital Wavelet Transform for Vertical Filter on Letter E, $m = 0$ Resolution

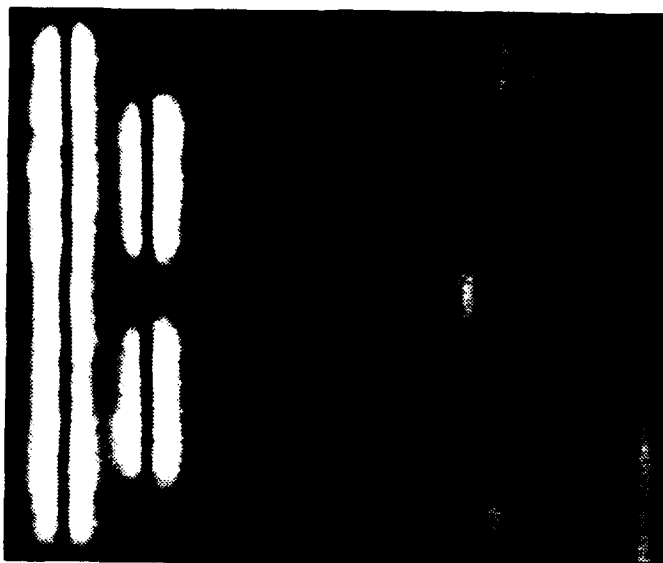


Figure 23. Optical Wavelet Transform for Vertical Filter on Letter E, $m = 1$ Resolution

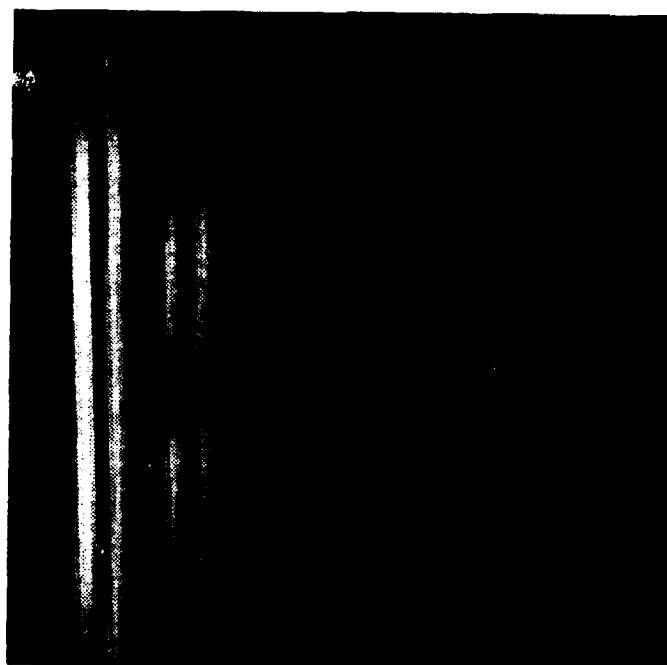


Figure 24. Digital Wavelet Transform for Vertical Filter on Letter E, $m = 1$ Resolution

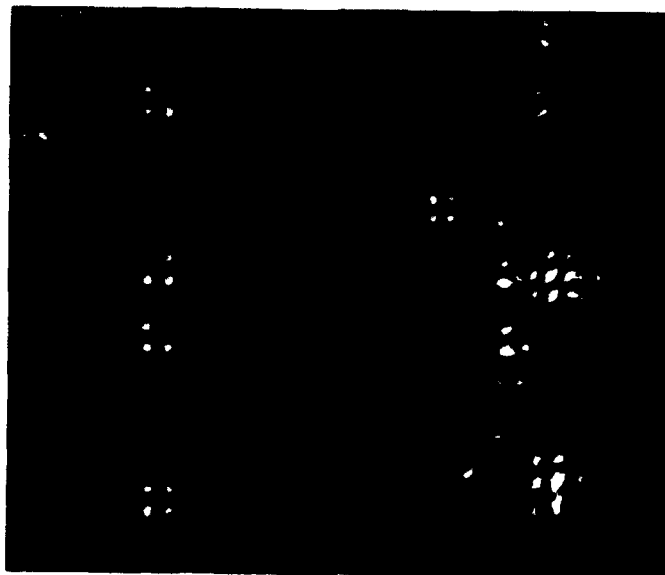


Figure 25. Optical Wavelet Transform for Diagonal Filter on Letter E, $m = 0$ Resolution

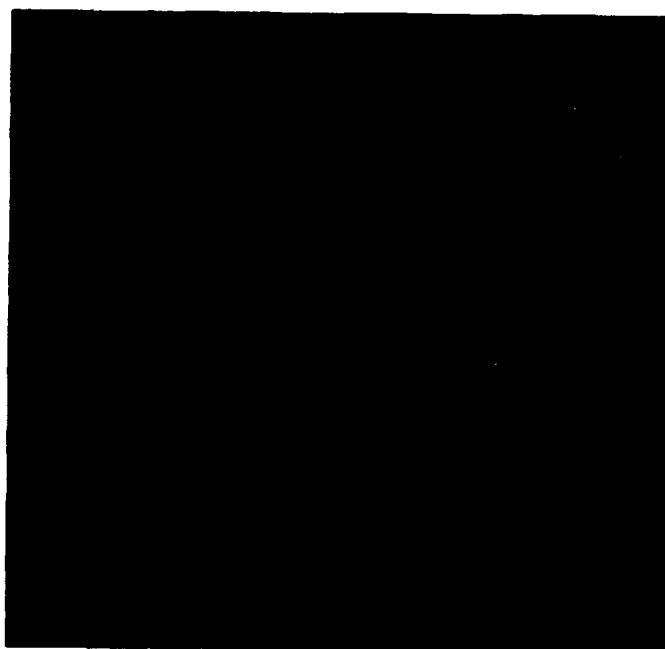


Figure 26. Digital Wavelet Transform for Diagonal Filter on Letter E, $m = 0$ Resolution

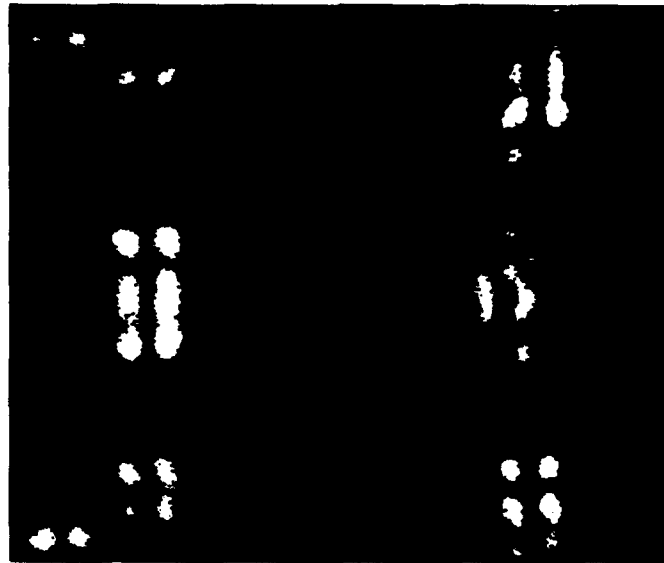


Figure 27. Optical Wavelet Transform for Diagonal Filter on Letter E, $m = 1$ Resolution

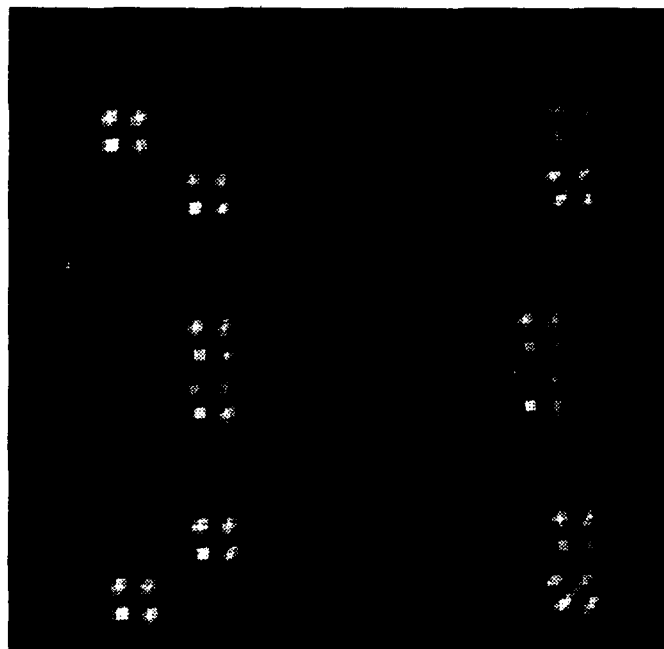


Figure 28. Digital Wavelet Transform for Diagonal Filter on Letter E, $m = 1$ Resolution

4.2 Optical Biorthogonal Wavelet Transform of Lenna

The image of Lenna was used in order to compare to results obtained in past research efforts at the Air Force Institute of Technology. The image of Lenna appears in this research because it contains significant complexity. The image contains detail at various resolution, optimal for exploitation using multiresolutional analysis. Past research efforts explored correlation with a Vander Lugt Matched Spatial Filter (MSF) of a Harr wavelet (25, 8) as well as correlation with a phase-only spatial filter of the Harr wavelet created using a computer generated hologram (2).

The image of Lenna was binarized and placed on the MOSLM. As before with the letter "E", the image of Lenna was captured at the output of the optical correlator shown in figure 3 with the wavelet filter removed from the setup. The image is shown in Figure 29. The image of Lenna was useful for exploring the wavelet transform because of the various levels of detail which exist at different scales in the image. Each of the three wavelet filters depicted in Figures 9-11 was applied to the image



Figure 29. Lenna

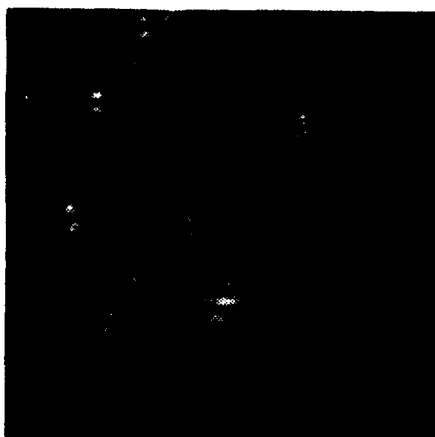
of Lenna with good results.

Each of the three wavelet filters was applied to the image. Results showed how the various image details were enhanced by each of the filters. In turn, three resolutional scalings of each wavelet were applied to the image of Lenna, through adjustment of the optical correlator configuration. This resulted in nine different wavelet transforms of the image of Lenna.

The three scalings of the horizontal wavelet are shown in Figure 30. The finest resolution horizontal wavelet represented the higher passband of spatial frequencies. The edges of the image represented the highest frequency components. The eyebrows, the mouth, and the brim of the hat were enhanced at this resolution. As the scaling factor was doubled, the effect was to allow some of the lower spatial frequencies to pass. More details from the hat and face were visible now. Other objects in the background became apparent. As the scaling was doubled again, the image details began to take on more form. The lines have been replaced with the low frequency components making up the shapes within the image. The three step transition between linear details and form was obvious with the vertical wavelet as well. In Figure 31 the vertical details; the edges of the nose, hair, and feathers, were the target. Again, as the scale of the wavelet was increased, more of the form became more prominent as the edges were left out. Finally with the diagonal wavelet, in Figure 32 the process was repeated. This time the shoulder, brim and crown of the hat, were enhanced in the image. Each of these nine images represented a unique resolutional detail for the image of Lenna. It was obvious from these results that the optical wavelet could be applied to the fingerprint to extract similar features. Features which could be used in the identification process.

4.3 Optical Biorthogonal Wavelet Transform of a Fingerprint

The same nine wavelet transforms were applied to a fingerprint image. This process revealed several levels of detail within the fingerprint, detail which could be exploited for recognition algorithms. The input image of the fingerprint was



(a)

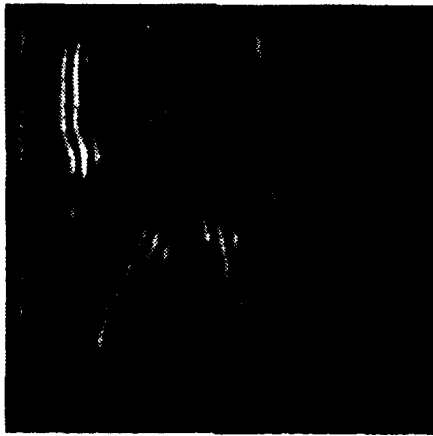


(b)



(c)

Figure 30. Horizontal Wavelet Transform Results for Lenna: (a) $m = 0$ (b) $m = 1$
(c) $m = 2$



(a)

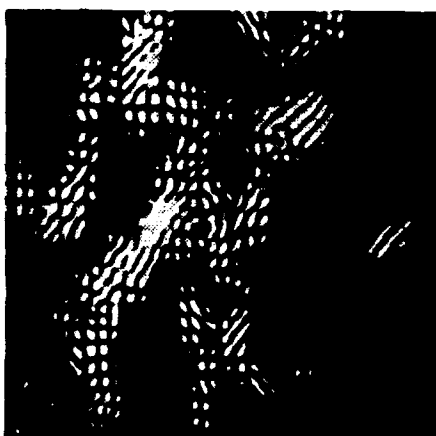


(b)



(c)

Figure 31. Vertical Wavelet Transform Results for Lenna: (a) $m = 0$ (b) $m = 1$ (c) $m = 2$



(a)



(b)



(c)

Figure 32. Diagonal Wavelet Transform Results for Lenna: (a) $m = 0$ (b) $m = 1$
(c) $m = 2$

binarized and placed on the MOSLM. The image of the fingerprint as captured through the CCD camera is shown on Figure 33. The fingerprint image consisted

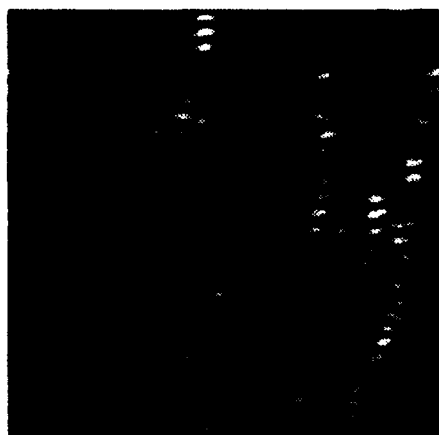


Figure 33. Fingerprint

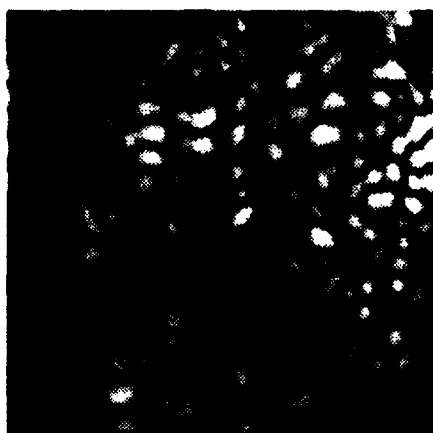
mainly of ridge lines. Since it was the structure of these lines which uniquely specified an individual's fingerprint, the wavelet filter was used to enhance the structure of these lines at various spatial frequencies. The fingerprint image was almost radial in structure, containing lines which had spatial frequencies in all three locations: horizontal, vertical, and diagonal. As before with the image of Lenna, each of the nine wavelet transformed images was unique. Of special interest was the results with the finest resolution diagonal wavelet transform in Figure 36(a). In this case there was plenty of energy in the diagonal frequencies, avoiding the problem experienced earlier with the letter "E" (see Figure 25).

To enhance the optical fingerprint identification process, the digital wavelet transform was applied to the fingerprint. The optical correlator identification process was limited by its rotational variance. To remedy this, the wavelet transform was used to enhance those features of the fingerprint that were rotational symmet-

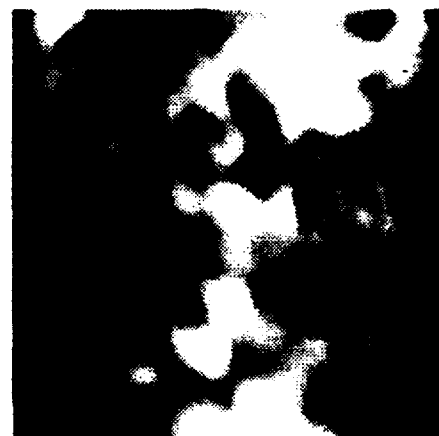
rical. Since the fingerprint was mainly radial in structure, the wavelet transform could be used to emphasize that radial structure for identification. The finest resolution diagonal wavelet transform was interesting because of two reasons. First, it contained a significant amount of energy. Energy which was required for creating the thermoplastic hologram in the identification stage. Second and more important, the diagonal wavelet transform enhanced the radial line structure in a way which approached rotational symmetry. This transform was chosen as the best candidate for the improved optical wavelet fingerprint identifier.



(a)

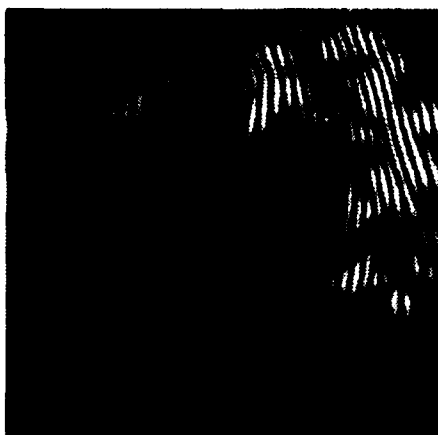


(b)

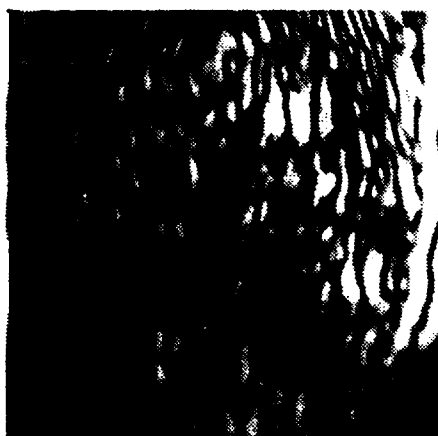


(c)

Figure 34. Horizontal Wavelet Transform Results for Fingerprint: (a) $m = 0$ (b) $m = 1$ (c) $m = 2$



(a)



(b)

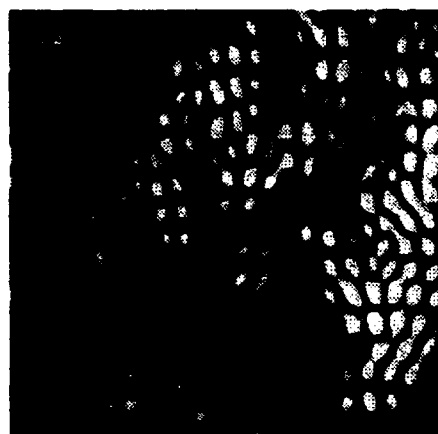


(c)

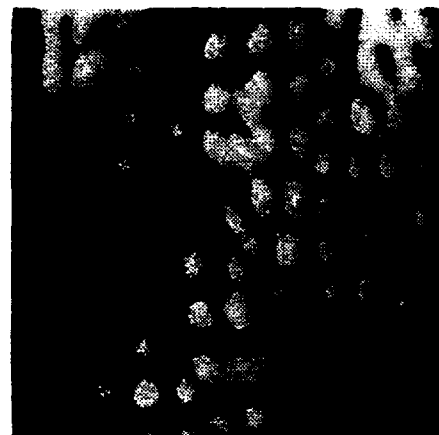
Figure 35. Vertical Wavelet Transform Results for Fingerprint: (a) $m = 0$ (b) $m = 1$ (c) $m = 2$



(a)



(b)



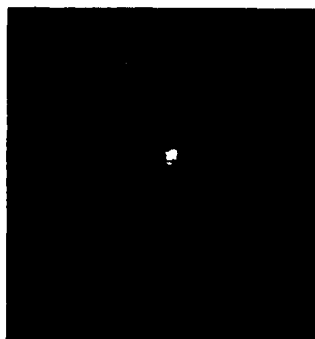
(c)

Figure 36. Diagonal Wavelet Transform Results for Fingerprint: (a) $m = 0$ (b) $m = 1$ (c) $m = 2$

4.4 Improved Optical Wavelet Fingerprint Identifier

A set of subjects was used for identification, the same set used in parallel personal identification research. These other research efforts involved speech, handwriting, and face recognition (26, 28, 19). The subjects placed their thumbprint on the prism in the optical arrangement portrayed in Figure 13. The computer generated hologram of the diagonal wavelet filter was used to enhance the diagonal features of the fingerprint by computing the wavelet transform of the print. This image was then correlated with a Vander Lugt MSF of a wavelet transformed print. The correlation peak was then analyzed to determine if this arrangement could discriminate between wavelet transformed fingerprints.

Results showed that the wavelet transformed fingerprint did indeed contain enough uniqueness to discriminate between fingerprints. The correlation peaks captured with the CCD camera are shown in Figure 37. A thermoplastic hologram was created using the first subject's print. The auto-correlation peak was captured with the print left on the prism after creating the thermoplastic hologram. Subject one then removed the thumb and subsequently returned the thumb to the prism, after it had been wiped clean. The resulting correlation peak was then captured and recorded as "subject-one correlation". Four other subjects were then used to match against subject one. The result was that the correlation peak was much more obvious for subject one. This proved that the wavelet transformed fingerprint, with its reduced feature set could still discriminate between fingerprints.



Auto-correlation



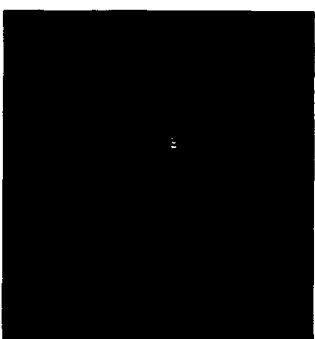
**Subject 1 Cross-correlation
With Subject 1 MSF**



**Subject 2 Cross-correlation
With Subject 1 MSF**



**Subject 3 Cross-correlation
With Subject 1 MSF**



**Subject 4 Cross-correlation
With Subject 1 MSF**



**Subject 5 Cross-correlation
With Subject 1 MSF**

Figure 37. Improved Optical Wavelet Fingerprint Identifier Results: Discrimination Against Subject 1 MSF

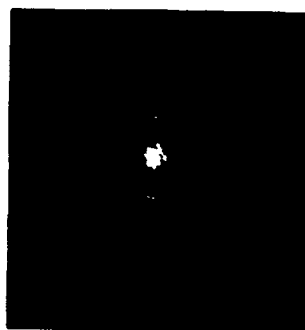
4.5 Test for Rotational Invariance

To determine if the wavelet transformed fingerprint added any rotational invariance to the Vander Lugt MSF, a comparison was made between the standard Vander Lugt MSF correlator and the wavelet process. A glass slide of a fingerprint was used as the input image. The glass slide was placed on a rotating stand which could measure the angular rotation in degrees. A MSF was created for both the normal and wavelet transformed non-rotated fingerprint. The auto-correlation peak was recorded. Then the glass slide with the print on it was rotated so that the effect of rotation could be observed and recorded. The results are shown in Figure 38, where the correlation peaks were captured for the normal and the wavelet transformed fingerprint. The correlation peaks for the offset results are plotted in Figures 40 through 45. The wavelet fingerprint displayed a greater amount of invariance to the rotation out to 5 degrees off center. The energy in the peak remained strong in direct contrast with the peak for the normal fingerprint. The wavelet correlation peak was strong enough in the 5 degrees offset so that discrimination was possible between the rotated fingerprint and a different on-axis print. To illustrate this, the 5 degree offset peak was compared to the results in Figure 37 for subject 2. As shown in Figure 39, the offset fingerprint was still distinctive from another subject. Even when the fingerprint was offset by as much as five degrees, the optical identifier was able to determine the identity. This adds flexibility to the optical identification process, allowing the subject some latitude when placing the print in the arrangement for identification.

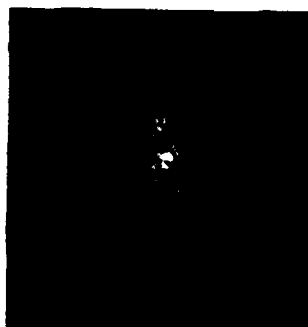
Comparison of the signal-to-noise ratio (SNR) for the correlation peaks in Figure 38 is shown in Table 2. The value for the SNR was determined by comparing the average value of the signal to that of the noise. To discriminate between signal and noise, the largest pixel value was determined. The signal was considered to be those pixel values within 3 dB of the peak. Everything else was considered to be noise.



Normal Autocorrelation



Wavelet Autocorrelation

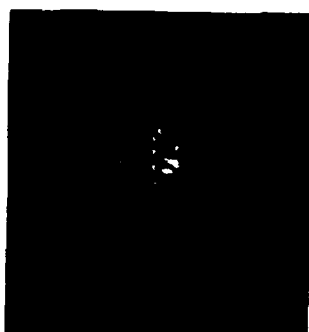


Normal Autocorrelation

3 Degree Offset



Wavelet Autocorrelation



Normal Autocorrelation

5 Degree Offset



Wavelet Autocorrelation

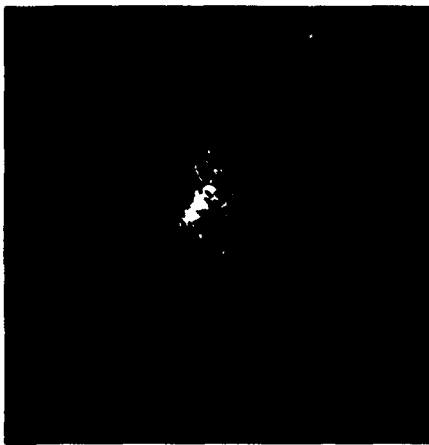
Figure 38. Auto-Correlation Peak vs Offset Rotation for Normal and Wavelet Transformed Fingerprint Image at Various Rotations

Offset	SNR Wavelet Correlator	SNR Normal Correlator
0°	51.34	49.72
3°	38.71	22.98
5°	40.5	20.74

Table 2. Signal-to-Noise Ratios for Various Offsets

The values shown in Table 2 were generated by comparing the average value of the signal peak to the standard deviation of the noise. As shown in equation 16, the average value of the noise was subtracted from the peak in order to reduce bias (20).

$$SNR = \frac{\bar{\mu}(Peak) - \bar{\mu}(Noise)}{\sigma(Noise)} \quad (16)$$



(a)



(b)

Figure 39. Comparison of (a) Five Degree Offset Wavelet Auto-correlation and (b) Non-Rotated Subject Two Wavelet Cross-correlation with Subject One

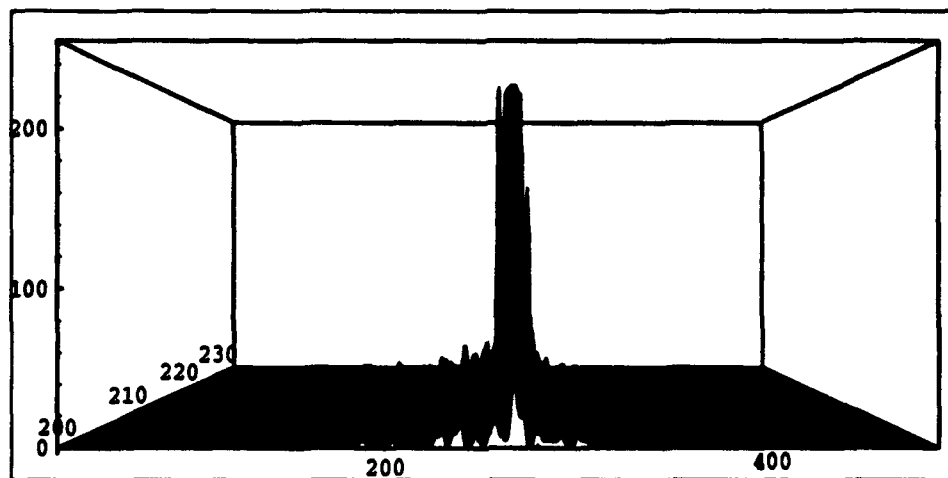


Figure 40. MSF Correlation Peak Plot for Normal Non-Rotated Fingerprint

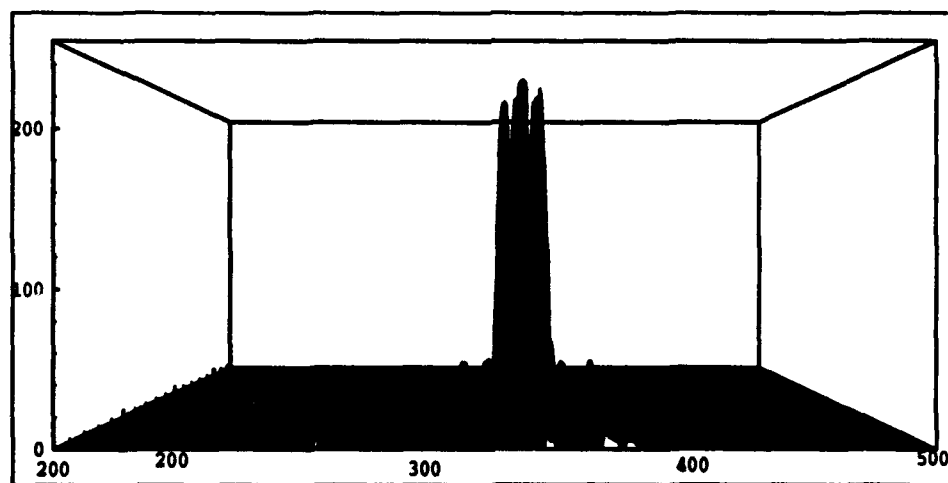


Figure 41. MSF Correlation Peak Plot for Wavelet Transformed Non-Rotated Fingerprint

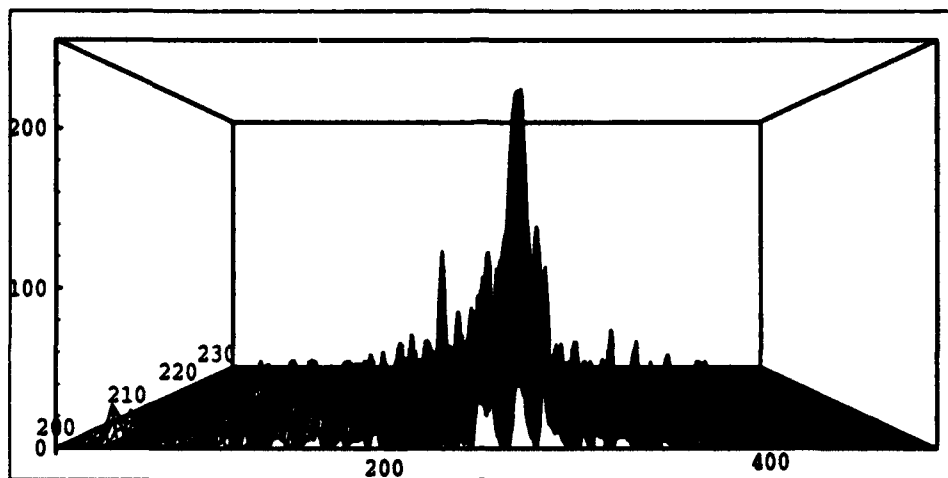


Figure 42. MSF Correlation Peak Plot for Normal 3 Degree Offset Fingerprint

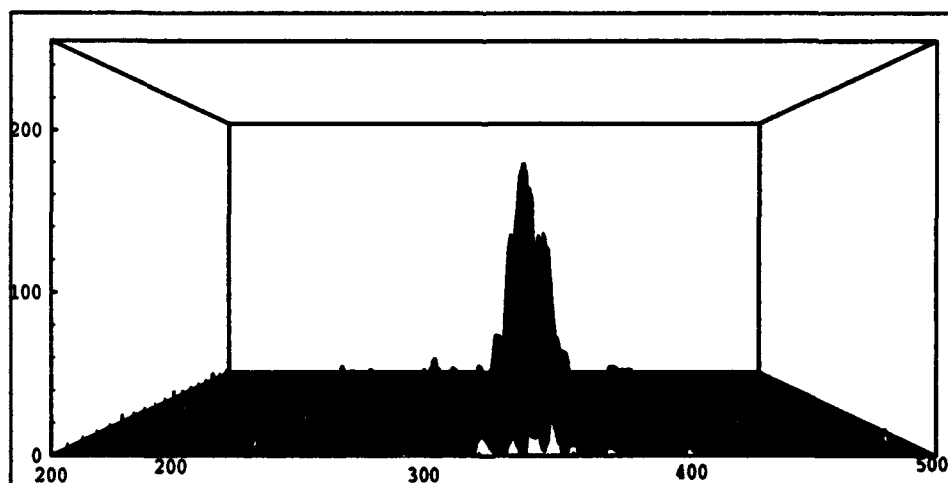


Figure 43. MSF Correlation Peak Plot for Wavelet Transformed 3 Degree Offset Fingerprint

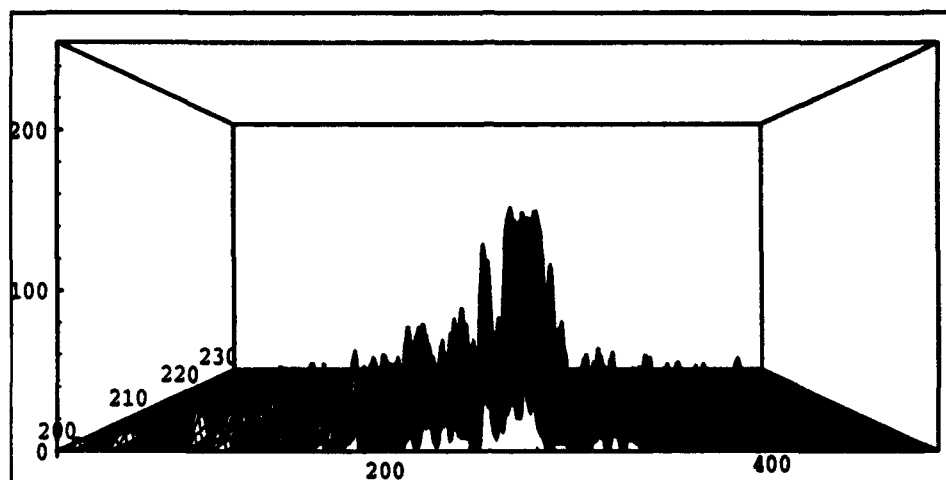


Figure 44. MSF Correlation Peak Plot for Normal 5 Degree Offset Fingerprint

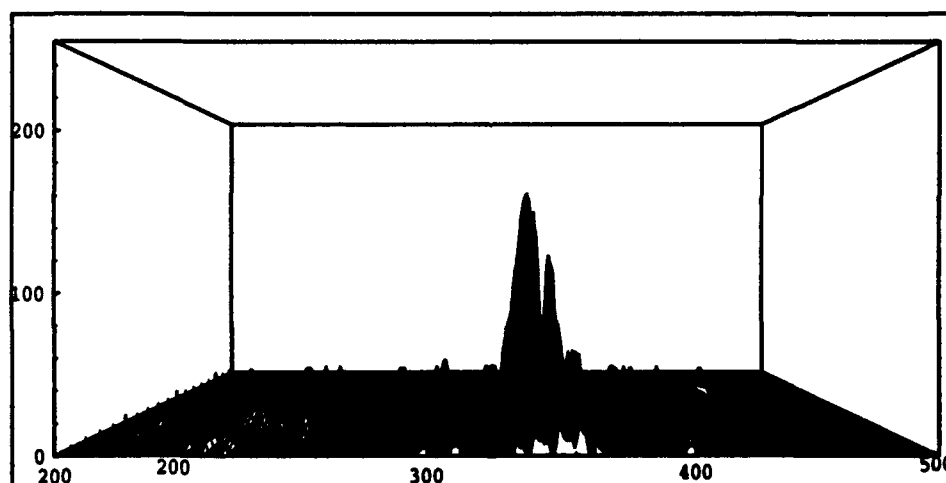


Figure 45. MSF Correlation Peak Plot for Wavelet Transformed 5 Degree Offset Fingerprint

4.6 Summary

This chapter showed the results of the biorthogonal wavelet transform on three input images. The results were compared to digital simulations and past research efforts. The wavelet transform was used to improve upon the optical fingerprint identifier. The results were favorable. SNR ratios for the wavelet transformed fingerprint showed a greater tolerance to rotational offsets than did the normal fingerprint. The next chapter draws conclusions and provides suggestions for future research.

V. Conclusions

This research implemented the optical wavelet transform for a symmetric biorthogonal wavelet function. The optical wavelet transform demonstrated distinct advantage over the computer based MRA algorithm. The optical process computed the wavelet transform in real-time with continuous shift variable. The scale variable of the wavelet transform was varied with continuous distribution through manipulation of optical arrangement. This was an advantage over the computer based technique which uses discrete, dyadic values for scale and shift variables.

A detour phase hologram of the two dimensional wavelet filters was constructed and operational. The optical wavelet transformed images compared well with digital methods. This optical method also showed improvement over past research in this area here at AFIT. The choice of the holographic technique and type of wavelet showed great promise.

The optical wavelet transform of a fingerprint added to the identification process. An optically transformed fingerprint image, a reduced feature set of the original, still demonstrated enough unique qualities for discrimination with an MSF. The wavelet transformed image also demonstrated an added rotational invariance when compared to a normal fingerprint image. This successful application of the optical wavelet transform gives hope to further study.

5.1 Future Applications

Using the optical wavelet transform for enhancing fingerprint identification would assist in the development of a field unit for scanning fingerprints. This application would benefit law enforcement agencies, allowing rapid storage, identification, and retrieval of fingerprint images, with the rotational invariance allowing some degree of flexibility when attempting to input a print. The enhanced fingerprint identification would also improve security access systems in remote locations.

The wavelet transform also shows promise for image segmentation. An optical process could be used in automatic pattern recognition for application in a smart weapon system. A system could be developed which could effectively scan for several resolutions, using those resolutions to discriminate between objects in a scene.

5.2 Recommendations

For continued research in optical wavelet transforms, the following areas should be further investigated:

1. A comparison of different wavelet functions for transforming fingerprint images should be made to understand how the choice of wavelet will affect the identification process.
2. Investigate the use of the optical wavelet transform in image segmentation for pattern recognition.
3. Demonstrate an optical process for decomposition and perfect reconstruction of an image.
4. A comparison of other magnitude and phase holographic techniques for creating the wavelet filter would determine the optimal method for limiting distortion.
5. And finally, access to a larger printer with similar resolution would allow a larger amount of phase quantization levels, limiting the major cause of distortion in the holographic process.

*Appendix A. C Program used to Create Detour Phase Computer
Generated Hologram*

```
#include <stdio.h>
#include <math.h>
#include "macros.h"

float *vector();
float **matrix();

main(argc,argv)
int argc;
char **argv;

{int x,y,i,j, temp, bxsz, temp1, temp2, bxht, bxwd;
float *rdata;
float **mac;
double pi, hmag, **magdata, *mag, **phasedata, *phase;
int number_cells,number_points;
FILE *magfile, *phasefile, *output_file, *magchk, *phschk;

number_points=2576;
number_cells=161;
pi=3.1516152654;

/* Allocate memory for the input files for magnitude and phase of wavelet filter */

magdata=dmatrix(1,number_cells,1,number_cells);
mag=dvector(1,number_cells);
phasedata=dmatrix(1,number_cells,1,number_cells);
phase=dvector(1,number_cells);

rdata=vector(1,number_points);

mac=matrix(1,number_points,1,number_points);

/* Output file for CGH data */

output_file = fopen("cgh" ,"w");
```

```

magfile=fopen("magcghpsi", "r");
phasefile=fopen("phasescghpsi", "r");
magchk=fopen("magchk", "w");
phschk=fopen("phschk", "w");

loop1i(number_cells)
{
fscanf(magfile, "%le", &mag[i]);
fscanf(phasefile, "%le", &phase[i]);

}

loop1i(number_cells)
{

loop1j(number_cells)
{

magdata[i][j]=mag[i]*mag[j];
phasedata[i][j]=phase[i]+phase[j];
fprintf(magchk, "%d \n", 2*(int)(magdata[i][j]*42.44/2));

if (phasedata[i][j]>pi)
{phasedata[i][j]=phasedata[i][j]-(2*pi);}
if (phasedata[i][j]<-pi)
{phasedata[i][j]=phasedata[i][j]+(2*pi);}
fprintf(phschk, "%d \n", (int)(floor(phasedata[i][j]*4/pi)));

}
}

for (y=1;y<=number_cells;y++)
{
for (x=1;x<=number_cells;x++)
{

{temp1=2*(int)(magdata[x][y]*42.44/2);}
{bxht=(int)((16 - temp1)/2);}
if (phasedata[x][y]<0)
{temp2=(int)(floor(phasedata[x][y]*4/pi));}
else

```



```

{temp2=(int)(ceil(phasedata[x][y]*4/pi));}
{bxwd=(int)((6 - temp2)/2);}

```

```

for (i = 16*y - 15; i<=16*y; i++)
    {for (j= 16*x - 15; j<=16*x; j++)
        {
            if (i>=16*y-15+bxht & i<16*y-15+bxht+temp1 & j>=16*x-11+temp2 & j<16*x-3+temp2
                {mac[j][i]=1.0;}
            else
                {mac[j][i]=0.0;}
        }
    } /* end of j loop */
} /* end of i loop */

```

```

} /* end x loop */
} /* end y loop */

```

```

for (i = 1908; i<=1956; i++)
    {for (j= 1280; j<=1296; j++)
        {mac[i][j]=1.0;
        }
    }
for (j = 1908; j<=1956; j++)
    {for (i= 1280; i<=1296; i++)
        {mac[i][j]=1.0;
        }
    }

```

```

printf("Values computed saving the data\n");
fflush(stdout);

```

```

for (y=1; y<=number_points; y++)
{
    for (x=1; x<=number_points; x++)
        {rdata[x]=(float)mac[x][y];}
    fwrite(rdata, sizeof(float), number_points, output_file);}

```

```
free_vector(rdata, 1, number_points);
free_matrix(mac, 1, number_points, 1, number_points);
free_dvector(mag, 1, number_cells);
free_dvector(phase, 1, number_cells);
free_dmatrix(magdata, 1, number_cells, 1, number_cells);
free_dmatrix(phasedata, 1, number_cells, 1, number_cells);
fclose(output_file);
fclose(magfile);
fclose(phasefile);
fclose(magchk);
fclose(phschk);

} /* end main */
```

Bibliography

1. Antonini, Marc, et al. "Image Coding Using Wavelet Transform," *IEEE Transactions on Image Processing*, 205-220 (1992).
2. Block, Peter G. *Optical Haar Wavelet Transforms Using Computer Generated Holography*. MS thesis, Air Force Institute of Technology (AU), Wright-Patterson AFB, OH, December 1992.
3. Bock, Brett D., et al. "Design Considerations for Miniature Optical Correlation Systems That Use Pixelated Input and Filter Transducers." *SPIE Optical Information-Processing Systems and Architectures II*. 297-309. 1990.
4. Bradley, Jonathan N., et al. "The FBI Wavelet/Scaler Quantization Standard for Gray-Scale Fingerprint Image Compression." Document LA-UR-93-1659.
5. Brislawn, Christopher M. "Classification of Symetric Wavelet Transforms." Document LA-UR-92-2823.
6. Brislawn, Christopher M. "WSQ Gray-scale Fingerprint Image Compression Specification."
7. Brown, B.R. and A.W. Lohman. "Complex Spatial Filtering with Binary Masks," *Applied Optics*, 967-969 (1966).
8. Burns et al. "Optical Haar Wavelet Transform," *Optical Engineering*, 1852-1858 (September 1992).
9. Cohen, et al. "Biorthogonal Wavelet Bases," *Communications in Pure Applied Math*, 474-521 (July 1992).
10. David P. Casasent and John-Scott Smokelin and Anqi Ye. "Wavelet and Gabor transforms for detection," *Optical Engineering*, 1893-1898 (September 1992).
11. Davis, Jeffrey A., et al. "Compact Optical Correlator Design," *Applied Optics*, 10-11 (1989).
12. Fielding, K.H., et al. "Optical Fingerprint Identification by Binary Joint Transform Correlation," *Optical Engineering*, 1958-1961 (December 1991).
13. Freysz, E., et al. "Optical Wavelet Transform of Fractal Aggregates," *Physical Review Letters*, 745-748 (1990).
14. F.T. Gamble and L.M. Frye and D.R. Grieser. "Real-time fingerprint verification system," *Applied Optics*, 652-655 (February 1992).
15. Hopper, T.E. "Grey-Scale Fingerprint Image Compression Status Report," *IEEE: Proceeds from Data Compression Conference*, 309-318 (1992).
16. Hopper, T.E., March 1993. FBI/Systems Technology Unit, Washington DC. Telephone Interview.

17. Ingrid Daubechies. *Ten Lectures on Wavelets*. Society for Industrial and Applied Mathematics, 1992.
18. J.W. Goodman. *Introduction to Fourier Optics*. McGraw-Hill Book Company, 1968.
19. Keller, John. *Identity Verification through the Fusion of Face and Speaker Recognition*. MS thesis, Air Force Institute of Technology (AU), Wright-Patterson AFB, OH, December 1993.
20. Kumar, B.V.K. Vijaya and D. Casasent. "Binarization effects in a correlator with noisy input data," *Applied Optics*, 1433-1437 (1981).
21. Li, Yao and Yan Zhang. "Coherent Optical Processing of Gabor and Wavelet Expansions of One- and Two-Dimensional Signals," *Optical Engineering*, 1865-1885 (1992).
22. Lugt, A.B. Vander. "Signal Detection by Complex Spatial Filtering," *IEEE Transactions on Information Processing, IT-10(2)*, 139-145 (1964).
23. Mallat, Stephane G. "A theory for multiresolutional signal decomposition: The wavelet representation," *IEEE Transactions on Image Processing*, 674-693 (1989).
24. Newport Corporation, Fountain Valley CA, "Operator's manual HC-300 Holographic Recording Device."
25. Pinski, Steven D. *Optical Image Segmentation Using Wavelet Correlation*. MS thesis, Air Force Institute of Technology (AU), Wright-Patterson AFB, OH, December 1991.
26. Prescott, D. Neale. *Speaker Identification Using Data Fusion with Auditory Models*. MS thesis, Air Force Institute of Technology (AU), Wright-Patterson AFB, OH, March 1994.
27. Ruskai et al. *Wavelets and Their Applications*. Jones and Bartlett Publishers, 1992.
28. Shartle, Gary. *Hand Written Word Recognition Based on Fourier Coefficients*. MS thesis, Air Force Institute of Technology (AU), Wright-Patterson AFB, OH, December 1993.
29. Sheng, Yunlong, et al. "Optical Wavelet Transform," *Optical Engineering*, 1840-1845 (September 1992).
30. Wai-Hon Lee. "Computer-Generated Holograms: Techniques and Applications," *Progress in Optics*, 223-243 (1978).
31. Wickerhauser, Mladen Victor. "High-Resolution Still Picture Compression," *Digital Signal Processing*, 2, 204-226 (1992).
32. W.J. Dallas. "Phase Quantization in Holograms-a Few Illustrations," *Applied Optics*, 674-676 (March 1971).

Vita

Captain Robert P. MacDonald was born on February 18, 1965 in Hartford, Connecticut. He graduated from Oliver Ames High School in Easton, Massachusetts in 1983. He received a four year Reserve Officer Training Corp scholarship to Worcester Polytechnic Institute from the Air Force, where he was awarded a Bachelor of Science degree in Electrical Engineering in 1987. For the eight months prior to coming on active duty, he worked as an Electrical Engineer at the Pilgrim Nuclear Power Station. After commissioning he was assigned to the Air Force Electronic Warfare Center (AFEWC) at Headquarters Electronic Security Command, Kelly AFB in San Antonio, Texas. He served there as an Electronic Warfare Systems Engineer for four and a half years. He entered the Electro-Optics program at the Graduate School of Engineering, Air Force Institute of Technology in May 1991.

Permanent address: 29 Berwick Rd
Easton, Massachusetts 02375

REPORT DOCUMENTATION PAGE			Form Approved OMB No. 0704-0188	
Public reporting burden for this collection of information is estimated to average 1 hour per response, including the time for reviewing instructions, searching existing data sources, gathering and maintaining the data needed, and completing and reviewing the collection of information. Send comments regarding this burden estimate or any other aspect of this collection of information, including suggestions for reducing this burden, to Washington Headquarters Services, Directorate for Information Operations and Reports, 1215 Jefferson Davis Highway, Suite 1204 Arlington, VA 22202-4302, and to the Office of Management and Budget, Paperwork Reduction Project (0704-0188), Washington, DC 20503.				
1. AGENCY USE ONLY (Leave blank)	2. REPORT DATE December 1993	3. REPORT TYPE AND DATES COVERED Master's Thesis		
4. TITLE AND SUBTITLE OPTICAL WAVELET TRANSFORM FOR FINGERPRINT IDENTIFICATION			5. FUNDING NUMBERS	
6. AUTHOR(S) Robert P. MacDonald				
7. PERFORMING ORGANIZATION NAME(S) AND ADDRESS(ES) Air Force Institute of Technology, WPAFB OH 45433-6583			8. PERFORMING ORGANIZATION REPORT NUMBER AFIT/GEO/ENG/93D-03	
9. SPONSORING / MONITORING AGENCY NAME(S) AND ADDRESS(ES)			10. SPONSORING / MONITORING AGENCY REPORT NUMBER	
11. SUPPLEMENTARY NOTES				
12a. DISTRIBUTION / AVAILABILITY STATEMENT Distribution Unlimited			12b. DISTRIBUTION CODE	
13. ABSTRACT (Maximum 200 words)				
<p style="text-align: center;">Abstract</p> <p>The Federal Bureau of Investigation (FBI) has recently sanctioned a wavelet fingerprint image compression algorithm developed for reducing storage requirements of digitized fingerprints. This research implements an optical wavelet transform of a fingerprint image, as the first step in an optical fingerprint identification process. Wavelet filters are created from computer generated holograms of biorthogonal wavelets, the same wavelets implemented in the FBI algorithm. Using a detour phase holographic technique, a complex binary filter mask is created with both symmetry and linear phase. The wavelet transform is implemented with continuous shift using an optical correlation between binarized fingerprints written on a Magneto-Optic Spatial Light Modulator (MOSLM) and the biorthogonal wavelet filters. A telescopic lens combination scales the transformed fingerprint onto the filters, providing a means of adjusting the biorthogonal wavelet filter dilation continuously. The wavelet transformed fingerprint is then applied to an optical fingerprint identification process. Comparison between normal fingerprints and wavelet transformed fingerprints shows improvement in the optical identification process, in terms of rotational invariance.</p>				
14. SUBJECT TERMS Wavelet Transform, Optical Information Processing, Optical Pattern Recognition, Computer Generated Holograms, Fingerprint Identification			15. NUMBER OF PAGES 68	
			16. PRICE CODE	
17. SECURITY CLASSIFICATION OF REPORT UNCLASSIFIED	18. SECURITY CLASSIFICATION OF THIS PAGE UNCLASSIFIED	19. SECURITY CLASSIFICATION OF ABSTRACT UNCLASSIFIED	20. LIMITATION OF ABSTRACT UL	